Judy Wu,* Maogang Gong, Russell C. Schmitz, Bo Liu

Abstract Colloidal semiconductor quantum dot/graphene van der Waals heterostructure nanohybrids are emerging technologies for photodetection. These nanohybrids combine advantages of the enhanced light-matter interaction and spectral tunability of quantum dots (QDs) and superior charge mobility in graphene, providing an affordable alternative for uncooled photodetectors with high gain or external quantum efficiency in a wide spectral range. In particular, the interfacing of QDs with high mobility graphene as a charge transport pathway has provided an effective resolution to the critical issue of charge transport in QD-only photodetectors stemming from the low charge mobility associated with both QD surface defect states and QD-QD junctions. Furthermore, the achieved capability in industrial-scale fabrication of graphene, colloidal QDs and QD/graphene nanohybrids has motivated efforts in researches of focal plane arrays that are expected to be not only high performance and low cost, but also light-weight, flexible and wearable. This chapter aims to provide an up-to-date review of the recent progress made in the research of QD/graphene nanohybrid photodetectors, together with a discussion on the challenges remaining and perspective in future research and development to make QD/graphene nanohybrids competitive for commercialization.

Keywords: Quantum dots · Graphene · Heterostructure · Nanohybrids · Photodetectors

1. Introduction

Since its discovery in 2004, graphene—a monolayer of carbon atoms arranged in a flat two-dimensional (2D) honeycomb lattice [8, 9]—has attracted enormous interest due to its superior physical properties including high charge carrier mobility, optical transparency, flexibility and

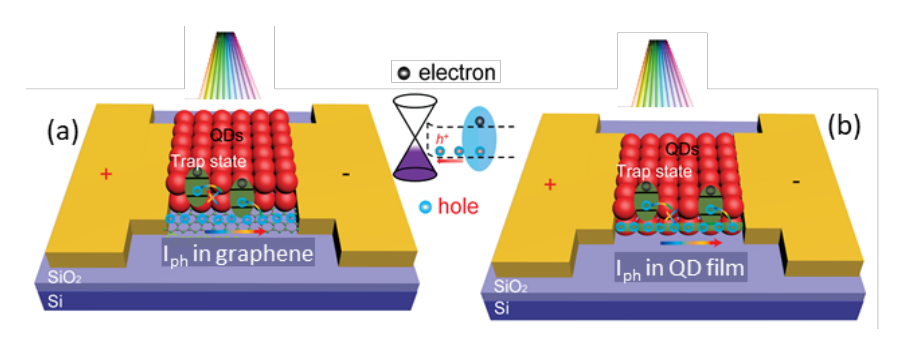
Judy Wu (corresponding author), Maogang Gong, Bo Liu Department of Physics and Astronomy University of Kansas Lawrence, KS 66045, USA Email: jwu@ku.edu

Russell C. Schmitz U.S. Army RDECOM CERDEC Night Vision and Electronic Sensors Directorate Ft. Belvoir, VA 22060, USA

chemical stability [8, 9]. In a larger scope, graphene belongs to the family of carbon nanostructures including fullerenes and carbon nanotubes (CNTs) which have won two Nobel Prizes and been the focus of intensive research and development in recent years [9, 13].

Graphene can be viewed as an atomically thin film available in large-area [17] and is compatible with conventional thin film-based microelectronics since the established microfabrication processes can be readily applied to make graphene circuits. This has motivated extensive exploration into graphene-based applications. Among these, optoelectronic nanohybrids involving graphene and quantum nanostructures have recently emerged as a unique scheme for high-performance photodetection [19-21]. The nanostructures are photosensitizers with morphologies of quantum dots (0D) [16, 20, 22-25], nanotubes and nanowires (1D) [26, 27], and nanosheets (2D) such as transition metal dichalcogenides (TMDC) [21, 28, 29]. The implementation of graphene of extraordinary charge carrier mobility in the nanohybrids makes a fundamental difference in the charge carrier transport in these nanohybrids optoelectronics as compared to the counterparts based on the nanostructures only.

Among other nanohybrids, colloidal quantum dots (QDs)/graphene van der Waals (vdW) heterostructures have recently emerged as a promising scheme for photodetectors [20], prompted by exciting progress made in colloidal QDs [32-48] and graphene [9, 13, 50-55]. It should be noted that the QD/graphene vdW heterostructure differs from the QD-only counterpart in charge transport. In fact, the QDs-only photodetectors (Fig. 1a) have been intensively studied, especially for infrared (IR) photodetection, in which the quantum confinement in QDs due to the suppressed phonon scattering [56] is expected to reduce dark current and hence improve the detector performance [57, 58]. This has been shown experimentally on colloidal HgTe QDs with surface passivation [59-61] and InSb-nanowires [62, 63]. However, the low carrier mobility, in the range of 10⁻⁶ cm⁻²V⁻¹s⁻¹ (in as-made HgTe QDs) to 10⁻⁴ cm⁻²V⁻¹s⁻¹ (with ligand exchange on HgTe QDs to passivate surface defects), remains a bottleneck to obtaining high detectivity (D^*) in QD-only photodetectors [61]. This bottleneck can be removed in QD/graphene vdW heterostructures by enabling charge transfer from QDs to graphene by the built-in electric field at the QD/graphene interface. Charge transport in graphene between the electrodes, as shown Fig. 1b, takes advantages of the high mobility (> 4×10^4 cm⁻²V⁻¹s⁻¹) in graphene at room temperature. After the first report of PbS QD/graphene photodetectors by Konstantatos et al in 2012 [20], many QD/graphene photodetectors have been explored and higher D* values, some by orders of magnitude compared to QD-only photodetectors, have been reported [5, 15, 20-22, 28, 29, 64-74]. Therefore, the QD/graphene vdW heterostructures may provide a unique scheme for high-sensitivity photodetectors by taking advantage of quantum confinement in semiconductor nanostructures and ballistic charge transport in graphene to enable unprecedented performance. This book chapter intends to provide a review of the recent progress made in research and development of the QD/graphene vdW heterostructures photodetectors including the fundamental physics underlying the optoelectronic process and key performance parameters (Section 2), processes developed for fabrication of colloidal QDs, graphene and QD/graphene vdW heterostructures (Section 3) and an overview of the current state-of-the arts performance of the QD/graphene vdW heterostructures photodetectors (Section 4). A summary of remaining challenges and future perspectives is given in Section 5.



 $\begin{tabular}{ll} \textbf{Fig. 1} Schematic of (a) QD/graphene vdW heterostructures (I_{ph} transfer in graphene), and (b) QD-only (I_{ph} transfer in QD-film) photodetectors. \\ \end{tabular}$

2. Background of QD/graphene van der Waals Heterostructures

The QD/graphene vdW heterostructure is a quantum device, taking advantage of the strong quantum confinement in QDs with enhanced light-matter interaction, spectral tunability, and suppressed phonon scattering [39, 75, 76], and of the extraordinary charge mobility of graphene at room temperature. [9, 13, 54, 55]. For photodetection, the QD/graphene vdW heterostructures can provide distinct advantages over their conventional semiconductor counterparts. First, the strong quantum confinement in ODs leads to much enhanced light absorption, spectral tunability much beyond the optical cutoff of bulk semiconductors, and reduced dark current due to suppressed phonon scattering. Second, a high external quantum efficiency (EQE) or photoconductive gain up to 10^{10} - 10^{12} can be enabled in various QD/graphene photodetectors, which results in high photoresponsivity and D^* [16, 20, 25]. Third, the Fermi level in graphene can be tuned by applying a gate voltage, shifting the Fermi energy of graphene with respect to the conduction and valence bands of the sensitizers for an optimal built-in field for exciton dissociation and charge transfer across the QD/graphene interface [20, 22]. Fourth, highly crystalline colloidal QDs can be synthesized with controllable dimensions, morphology and chemical composition using low-cost, non-/low-vacuum processes. This provides an additional advantage towards commercial applications and allows integration with Si-based readout circuits (Si-ROIC) using inkjet printing of the QD sensitizers [26, 77-79]. Finally, the high mechanical strength of a single sheet of graphene allows transfer of graphene onto various functional substrates, including Si-ROIC and flexible substrates with predefined electrodes. Unlike most other carbon-based nanostructures, the two-dimensional (2D) nature of graphene would allow most established lithography approaches for microfabrication and nanofabrication of electronic circuits to be applied to graphene, conferring benefits such as being monolithic, flexible, wearable, etc. to various commercial applications [28, 80, 81].

2.1. Graphene

Monolayer graphene has perfect crystallinity and extraordinary physical properties including unique electronic structure, high carrier mobility, optical absorption and mechanical strength [13, 50-55]. From an electronic structure point of view, graphene is a gapless, relativistic (E_g =0) semiconductor or semimetal [82], which means the charge carriers (both electrons and holes) can be described by a linear dispersion of $E = \hbar v_F k$, where the momentum-independent Fermi velocity, v_F , is as high as 1/300 of the speed of light. This results in high carrier mobility (μ) that seems independent of temperature in a large range, independent of applied electric field, and is comparable for holes and electrons [51]. Experimentally, high μ up to~15,000 cm²·V⁻¹·s⁻¹ has been observed on exfoliated graphene for both electrons and holes in the temperature range of 10-

100 K, which could be further improved by eliminating extrinsic charge scatting mechanisms and defects in graphene. The intrinsic acoustic phonon limit of mobility is projected to be $\sim 200,000$ cm²/V·s⁻¹ at room temperature assuming a carrier density of $(n) \sim 10^{12}$ cm⁻² at the charge neutrality or so-called Dirac point [51, 55]. It should be pointed out that the carrier mobility in graphene is higher by many orders of magnitude than in metals and most semiconductors at room temperature. For example, the electron and hole mobility for Si at room temperature are around 1400 cm²·V⁻¹·s⁻¹ and 450 cm²·V⁻¹·s⁻¹, respectively.

Intrinsic graphene has a zero energy bandgap E_g [51], which has prevented its use in a similar way to conventional semiconductors of well-defined E_g . Graphene absorbs incident light via interband transitions and exhibits a flat absorption $A=\pi\alpha\approx 2.3\%$ or transmittance T=I-A=97.7% (the fine-structure constant $\alpha=e^2/(4\pi\epsilon_0\hbar c)=G_0/(\pi\epsilon_0 c)\approx 1/137$) per graphene sheet in broadband from near ultraviolet to mid-infrared [82-85]. This absorption is one of the largest of all known materials (per atomic sheet). The low n and high μ in graphene imply that graphene can be an excellent alternative [81] to conventional transparent conductors [86] broadly employed for a large variety of photonic and optoelectronic applications [80, 87] including flexible displays, light emitting devices [88], photodetectors [89], touch screens, transistors [8, 90], electromechanical resonators [91], ultracapacitors [92] and photovoltaics [93]. In addition to high electrical conductivity and optical transparency in a wide spectral transmission window with the lower frequency cutoff proportional to n [94, 95], graphene has additional advantages of flexibility, low cost, light weight, and a favorable work function of ~4.42 eV comparable to many metals for many other optoelectronic applications [81, 96-100].

2.1.1. Graphene as Photosensitizers

Graphene-based optoelectronics have emerged as an important area with graphene as either the active or the electrode material. In the former, graphene photodetectors have been demonstrated with high frequency photodetection up to 40 GHz [9, 80, 89, 101]. However, the photoresponsivity has been limited by the low optical absorption of 2.3% in monolayer graphene [82] and lack of a high photoconductive gain mechanism. In the latter, sensitizer/graphene nanohybrids including QD/graphene vdW heterostructures enable enhanced photoresponse using nanostructure photosensitizers. **Fig. 2** illustrates a few examples.

Graphene-only photodetectors can be used in a wide optical spectrum from ultraviolet (UV) to Mid-IR due to the broad absorption of graphene via intra-band excitation. These photodetectors have shown to have high response speed, despite a limited photoresponsivity due to limited light absorption of 2.3% per graphene sheet (Fig. 2a). Taking 550 nm light as an example, the upper limit of the photoresponsivity for monolayer graphene is ~ 17 mA/W, assuming 100% EQE. In order to enhance the responsivity, various metallic plasmonic nanostructures have been implemented in graphene photodetectors for enhanced light absorption (Fig. 2b). nanoribbons (GNRs) and graphene quantum dots (GQDs) have also been explored to induce bandgaps (E_g) in graphene to enhance its light absorption. In both GNRs and GQDs, E_g appears when the dimension of GNRs and GQDs are reduced to <10 nm, while graphene is originally a semimetal with zero E_g . The E_g for GNRs due to the quantum confinement along the width of the GNRs is in the sub-eV or IR spectral range [102, 103] while that for the GQDs, with quantum confinement over all dimensions in the similar range of a few nm, is in the UV spectral range. In particular, the E_g can be tuned in both GNR and GQD cases by varying these dimensions in the range of 3-10 nm, providing unique tunability of optical spectra in IR (GNRs) or UV (GQDs), respectively. Figs. 2c-d illustrate examples of photodetectors employing GNRs and GODs. respectively,

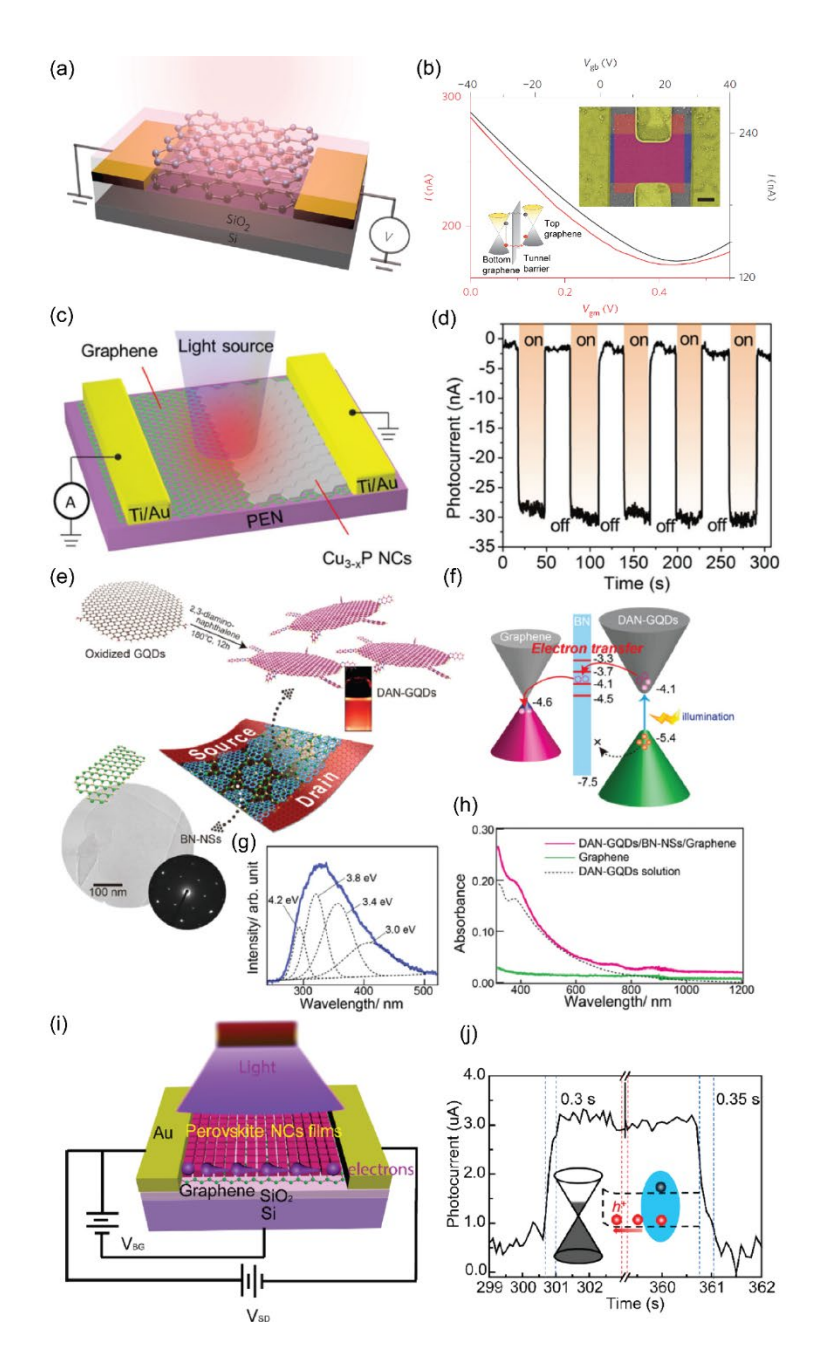


Fig. 2 (a) Schematic of graphene double layer heterostructure photodetectors. (b) Current curve for bottom graphene layer using silicon back gate (black) and top graphene layer using the bottom graphene as the gate (red). Reproduced with permission.[1] Copyright 2014, Nature Publishing. (c) Schematic diagram of the graphene-localized surface plasmon resonance (LSPR) Cu_{3-x}P nanocrystal (NC) heterojunction photodetectors on polyethylene naphthalate (PEN) substrate. (d) Dynamic photocurrent response excited under 1550 nm light illumination. Reproduced with permission.[3] Copyright 2017, John Wiley and Sons. (e) Schematic image of a Diaminonaphthalene-functionalized graphene quantum dots/boron nitride nanosheets@graphene field effect transistor (DAN-GQD/BN-NS@GFET) hybrid photodetector. (f) The band energy alignment of the photo-doping effect under illumination. (g-h) Cathodeluminescence spectrum of the BN-NSs and UV-Vis-NIR absorption spectra of graphene and the DAN-GQD/BN-NS/graphene film. Reproduced with permission.[14] Copyright 2008, Royal Society of Chemistry. (i) Schematic of CsPBCl₃ NCs/GFET hybrid photodetectors under UV illumination. (j) Time domain photoresponse of the CsPBCl₃ NCs/GFET device under the 400 nm light excitation. Reproduced with permission.[5] Copyright 2019, American Chemistry Society.

2.1.2. Graphene as Charge Transport Channel

In QD/graphene vdW heterostructure photodetectors, charges will transfer from QDs to graphene with graphene serving as the charge transport channel. This means that the OD/graphene vdW interface plays a critical role in facilitating the charge transfer shown in Fig. 1b [2, 20, 104-106]. In most of the QD/graphene vdW heterostructure devices, there are no purpose-generated chemical bonds between QD and graphene due to the 2D nature of the graphene. However, the vdW bonding is typically weak and hence can be easily affected by interface adsorbates from air and chemicals used in device fabrication. In addition, the electronic and optical behaviors of graphene are highly dependent on the interface including both OD/graphene and graphene/substrate interfaces [107, 108]. A direct consequence of a poor interface is increased carrier scattering and hence reduced carrier mobility in graphene. Moreover, the exciton dissociation into electrons and holes, and the follow-up charge transfer across the QD/graphene interface, can be dramatically degraded by a poor interface with a less effective built-in electric field and interface charge traps [22, 26, 71, 104, 106]. This makes controlling the QD/graphene vdW interface crucial to realizing the high photoresponse and high response speed. Many interesting works have focused on interface engineering to achieve high-performance QD/graphene vdW heterostructure photodetectors by optimizing charge transfer to and within graphene (see a more detailed discussion in Section 3.3).

Interface engineering can improve the performance of QDs/graphene photodetectors. As shown in Fig. 2e-2h, a BN-NS buffer layer is inserted at the NGQD/BN-NS layer interface, which facilitates transport of photoexcited electrons from the DAN-GQD photon absorber layer to graphene and block the photoexcited holes remaining in the NGQD layer. This DAN-GQD/BN-NS@GFET hybrid photodetector displayed high photoresponsivity of 2.3 × 10⁶ A/W and detectivity of 5.5×10¹³ Jones in the deep ultraviolet region at a fixed bias of 1V.[14] A more general and useful surface/interface engineering technique has been developed in recent years. Fig. 2i-2j shows a method of passivating crystalline CsPbCl₃ NCs surface with 3-mercaptopropionic acid (MPA), achieving superior ambient stability. Besides the ambient stability, this ligand-exchange and passivating technique improves the surface charge trap states of NCs and facilities high charge transfer efficiency between CsPbCl₃ NCs and graphene. Remarkable optoelectronic performance was achieved on the CsPbCl₃ NCs/graphene photodetector with a high responsivity of 10⁶ A/W, a high detectivity of 2×10¹³ Jones, a fast photoresponse time of 0.3 s and long term ambient stability of 2400 h.[5]

2.2. Semiconductor Quantum Dots

2.2.1. Band Tunability by QD Size

The strong quantum confinement in semiconductor QDs or NCs leads to advantages not only in the high photoconductive gain in the QD/graphene vdW heterostructures, to be discussed in **Section 2.3.1**, but also in the tunability of the spectral range through control of their shape, dimension, functionality (core/shell QDs), and carrier doping [94]. The bandgap dependence on the QD's size and shape can be expressed as [109]:

the QD's size and shape can be expressed as [109]:
$$E_{QD} = E_{bulk} + \frac{2h^2}{d^2} \left(\frac{1}{m_e} + \frac{1}{m_h} \right) - \frac{3.6e^2}{4\pi\varepsilon\varepsilon_0 d}$$
 (1)

where, E_{QD} is the bandgap of the QDs, E_{bulk} is the bandgap of corresponding bulk materials, h is the Planck's constant, d is the diameter of the QDs, m_e and m_h are the effective masses of electron and hole respectively, and e is the electron charge. The second and third term of the Eq. (1) represent the quantum confinement effect and coulomb interaction respectively. As shown in **Fig.** 3a, the absorption spectral can be tuned by the size of QDs, which is directly related to the tunable

bandgap of the QDs [4]. In addition, the bandgap of the QDs can also be tuned in a broad range by varying their chemical composition. For example, the absorption spectral of all-inorganic metal-halide perovskites CsPbX₃ NCs can cover the entire visible range by changing the elements X (Cl, Br, I) as shown **Fig. 3b** [6].

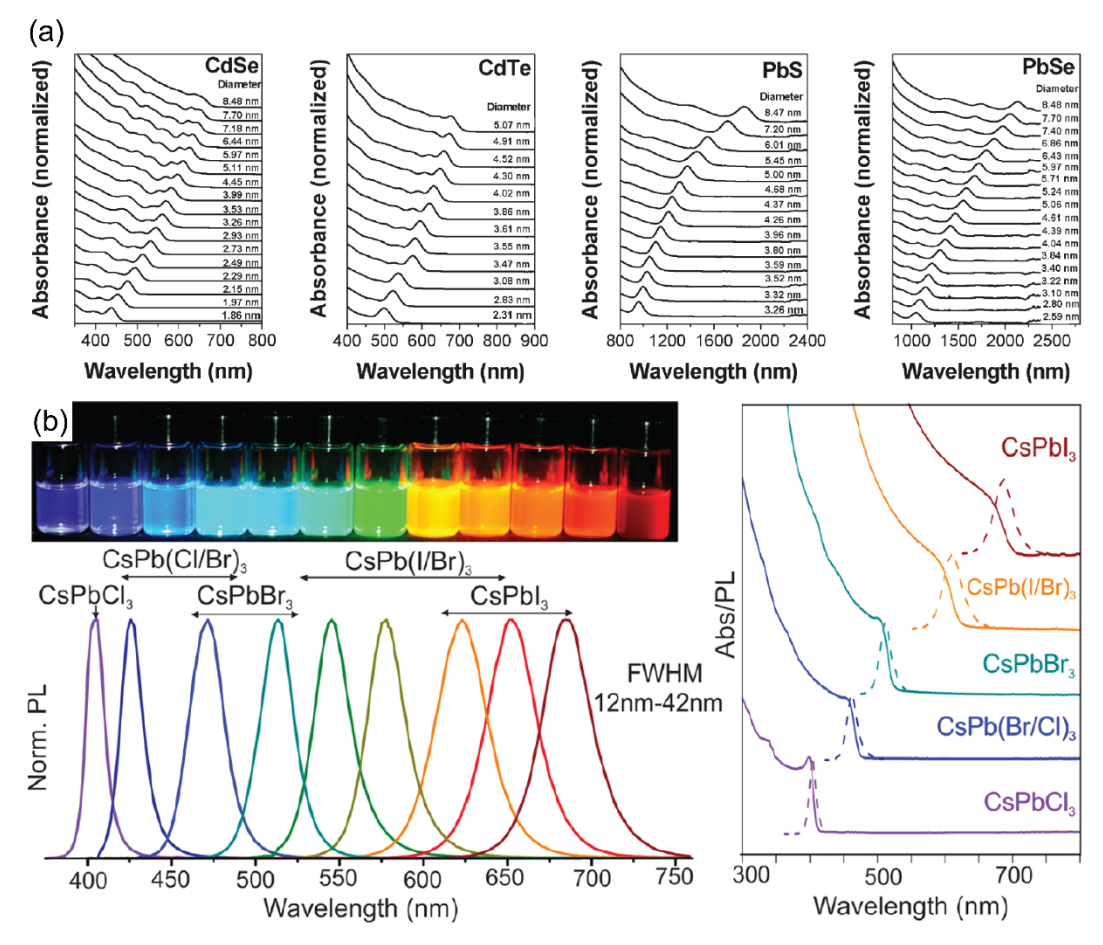


Fig. 3 (a) The size dependent optical absorption spectra of CdSe, CdTe, PbS and PbSe QDs. Reproduced with permission.[4] Copy right 2011, American Chemical Society. (b) Metal halide perovskite CsPbX₃ (X=Cl, Br, I) NCs exhibit composition tunable bandgap energies covering the entire visible spectral region. Reproduced with permission.[6] Copy right 2015, American Chemical Society.

2.2.2. Localized Surface Plasmonic Resonance for Enhanced Light Absorption and Spectral Tunalibity

Localized surface plasmonic resonance (LSPR) induced directly on nanostructure sensitizers via carrier doping, or in other plasmonic nanostructures placed in proximity of the sensitizer/graphene nanohybrids, could provide a light-trapping effect to enhance the photoresponse and shift the spectral range via exciton-plasmon coupling (**Fig. 4**) [72-74, 80, 89, 94, 110-113]. In the former, the light wavelength selectivity could be determined by the LSPR frequency of the plasmonic sensitizers, providing a viable wavelength tuning mechanism [94]. The LSPR frequency may be tuned by n- or p-doping of semiconductors of reasonable bandgaps that are large enough to not contribute a substantial dark current at room temperature [94]. Recently, Gong *et al* reported a broadband photosensitizer based on FeS₂ nanocubes that demonstrate strong LSPR effect

illustrated by the enhanced absorption and widened spectral range covering the UV-Visible-SWIR (SWIR regards short-wave IR) broadband (Figs. 4a-4c) [7, 105]. This LSPR FeS₂/graphene nanohybrid photodetector exhibits an efficient broadband photoresponse, with responsivities reaching 1.08×10⁶ A/W in the whole UV-Visible-SWIR range at a low operational voltage of 0.1 V. Besides doping semiconductor nanocrystals to produce LSPR for broadband and enhanced absorption, metal/semiconductor core/shell structure design is another efficient way to improve the light absorption at a limited active shell thickness with low absorption capacity. A template modulated colloidal approach for synthesizing metal core (AuCu) and metal-halide perovskite shell (CsPbCl₃) nanocrystals was reported as shown in Figs. 4d and 4e [15]. Enhanced light absorption was observed in the CsPbCl₃ shell with thickness of 2-4 nm, ascribed to the LSPR AuCu core with an average diameter of 7.1 nm. The LSPR AuCu core-induced light absorption of the perovskite shell enabled a remarkable 30 times-enhanced photoresponse in core/shell perovskite ODs/graphene nanohybrid photodetectors, compared to the counterparts with perovskite-only QDs. Plasmonic metal nanostructures may be placed in proximity of the nanohybrids photodetectors for the benefit of light trapping, which can be quantified using Finite-Difference Time-Domain (FDTD) simulation, and enhanced light absorption in QDs [112]. A recent work by Alamri et al [30] combined the plasmonic effects from TMD nanodiscs grown on graphene and Ag nanoparticles (AgNPs) using an in vacuo process, producing a seven-fold enhanced photoresponse (Figs. 4f-4h).

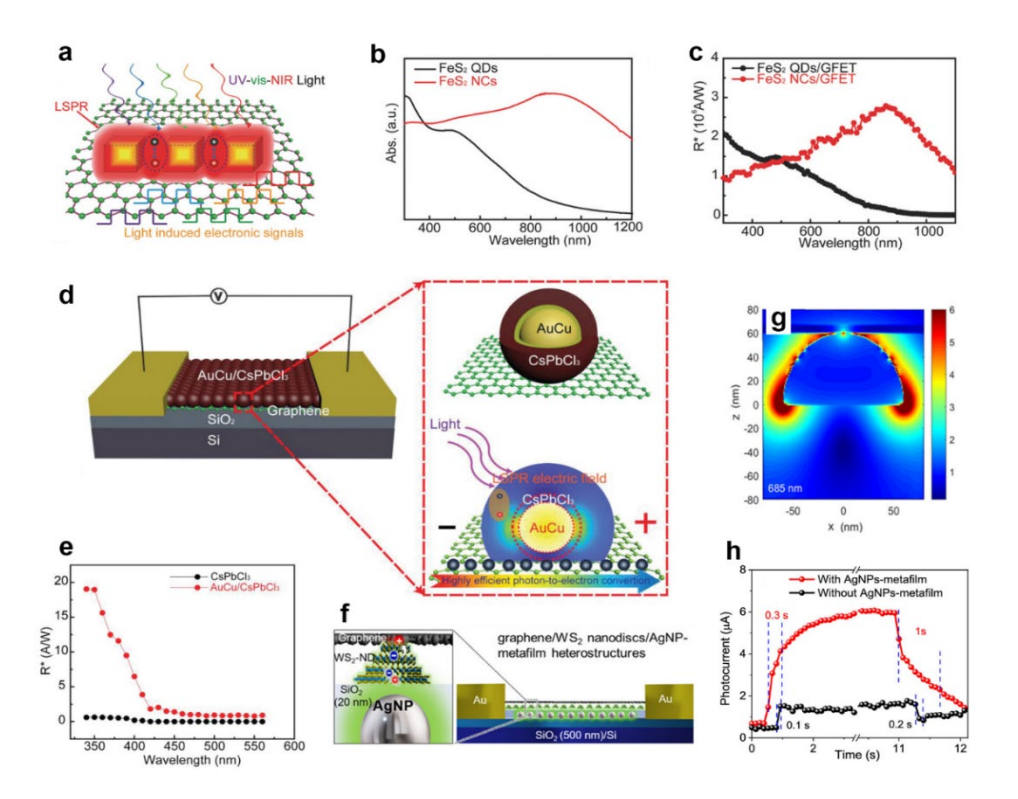


Fig. 4 (a) Diagram of localized surface plasmon resonances of FeS2 NCs and broadband photoresponse. (b) UV–vis–NIR absorption spectra of FeS2 QDs (black) and NCs (red). (c) spectral photoresponsivity of FeS₂ QDs/GFET (black) and FeS₂ NCs/GFET (red) devices. Reproduced from Ref.[7]. Copyright 2018, John Wiley and Sons. (d) Schematic image of AuCu/CsPbCl₃ core/shell/graphene hybrid photodetectors with LSPR enhanced photoresponsivity. (e) Spectral photoresponsivity measured on AuCu/CsPbCl₃ core/shell/graphene hybrid photodetectors and CsPbCl₃/graphene counterpart. Reproduced from Ref.[15]. Copyright 2020, John Wiley and Sons. (f) Schematic illustration of the graphene/WS2-ND/AgNP-metafilm heterostructure photodetector (g) FDTD simulated electromagnetic field mode profiles of a AgNP with r = 60 nm. (h) Photocurrent response of the photodetectors with (red) and without (black) the AgNP-metafilm at 450 nm and light intensity of 0.15 mW/cm² under 0.8 V bias. Reproduced from Ref. [30] Copyright 2020, American Chemical Society.

2.3. Optoelectronic Properties of QD/Graphene vdW Heterostructures

2.3.1. Photoconductive Gain

In the QD/graphene vdW heterostructures, the QD photosensitizers absorb incident light, and the excitons generated in QDs could be dissociated by the build-in electric field at the QD/graphene interface, followed by charge transfer to graphene driven by the built-in field. The photoresponse is literally a photo-gating effect on graphene measured from the source and drain electrodes. High EQE or photoconductive gain up to 10^{10} - 10^{12} can be achieved in QD/graphene vdW heterostructures photodetectors (**Fig. 5**). The gain is defined as: gain= τ_c/τ_t [20-22, 71, 106, 114],

where τ_c is the exciton life time in QDs and τ_l is the carrier transit time defined as: $\tau_l = l^2/\mu_c V_{bias}$. In a graphene channel of length l at a given source-drain bias voltage of V_{bias} , τ_l is inversely proportionate to the charge mobility μ_c in graphene [115]. Thus the high EQE or gain in the QD/graphene devices is a combination of the strong quantum confinement effects in QDs (high

 τ_c) and in graphene (low τ_c due to high mobility μ_c) [54, 55], which has been demonstrated in various QD/graphene photodetectors [5, 15, 20, 21, 28, 29, 65-69].

Achieving high gain is crucial to a high detectivity (D^*) . Specific detectivity D^* is a sample area-independent figure of merit which is used to compare the performance of different photodetectors, and is defined as

$$D^* = \frac{(A.\Delta f)^{1/2}}{NEP}$$

where A is the active area of a photodetector, Δf is the bandwidth, and noise equivalent power (NEP) is the minimum power that can be detected by the photodetector. NEP is expressed mathematically as $NEP = \frac{I_{noise}}{R}$, where the numerator I_{noise} is the noise current in a photodetector. Thus D^* can be further rewritten in terms of R as:

$$D^* = \frac{(A.\Delta f)^{1/2}}{I_{noise}} \cdot R$$

Since R is the ratio of photocurrent I_{ph} and incident light power P_{in} , and I_{ph} is proportional linearly to the gain, high gain in the photodetector will lead to a high D^* . In particular, high $D^* \sim 10^{11} - 10^{12}$ Jones, 10^{16} Jones, and $10^{13} - 10^{14}$ Jones has been demonstrated in uncooled near-IR (wavelength up to 1.55 µm), visible (400 nm - 700 nm) and UV detections (300 nm - 400 nm), respectively. [2, 5, 16, 20, 25, 116].

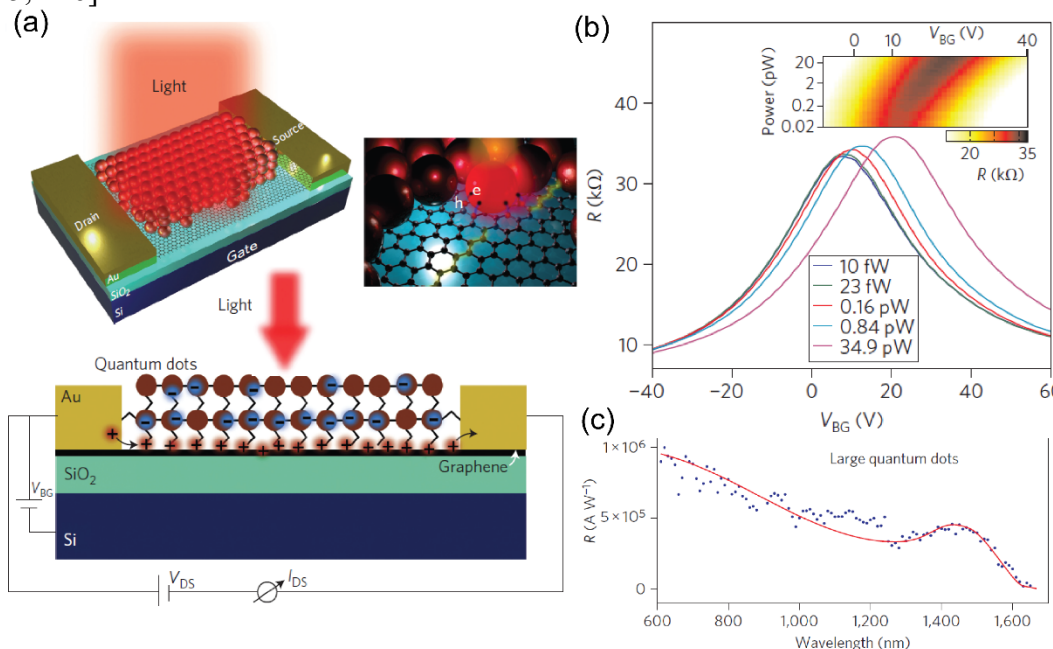


Fig. 5 (a) Schematic image of PbS QDs/graphene hybrid photodetectors, and the exciton production, separation and charge transfer process. (b) Graphene channel resistance as a function of back-gate voltage under different illumination intensities. The inset shows two-dimensional plot of graphene resistance as a function of optical power. (c) Spectral responsivity of this hybrid photodetectors. The spectral sensitivity of the device is dependent on the absorption spectra of the PbS QDs and can be easily tuned by controlling the QDs size. Reproduced with permission.[12] Copyright 2012, Springer Nature.

2.3.2. QD/graphene Interface Engineering

Considering that the physical properties of graphene can be affected by the interface between graphene and other materials, including QDs and supporting substrates, engineering such interfaces is crucial to the performance of the QD/graphene vdW heterostructure photodetectors. For example, an atomically thin Zn acetate or Zn(Ac) layer on the ZnO QDs can completely block the charge transfer from ZnO QDs to graphene and lead to negligible photoresponse to UV light. When this surface layer is systematically removed, improved photoresponse by orders of magnitude can be obtained [2]. In fact, many approaches have been developed to achieve clean vdW interfaces efficient for charge carrier transfer and with minimal carrier scattering for high mobility of carriers in graphene. Post-cleaning of the OD/graphene vdW interface in vacuum provides a convenient scheme in practical applications [106, 117]. For example, in the GaSe QD/graphene photodetector, the GaSe QDs printed onto the graphene channel often form an interface that may be contaminated by various chemicals, solvents and even air molecules used in the processing and printing of the GaSe ODs. This interface effect is demonstrated in the orders of magnitude improved dynamic photoresponse aftervacuum interface cleaning, enabling high gain up to 10^7 - 10^8 , visible detectivity D^* up to 7×10^{13} Jones and response time of 10-12 ms for rise and fall time [106]. This vacuum annealing method is, however, time consuming and may not be practical since many devices may need to be operated in non-vacuum environments. Ligand exchange provides an effective approach to passivate QD surface states and form an efficient charge transfer pathway from QD to graphene [2, 20, 104]. For example, Octon et al adopted a mixture of thioglycerol (TGL) and 2,3-dimercapto-1-propanol (DGT) to modify PbS QDs, leading to superior photoresponsivity up to 10⁹ A/W in PbS QD/graphene photodetectors, benefiting from the short length capping ligands and improved interface between PbS QDs and graphene [118]. Gong et al. replaced oleic acid and oleylamine with 3-mercaptopropionic acid (MPA) ligands in the fabrication of CsPbCl₃ QDs/graphene hybrid photodetectors to improve the stability of the CsPbCl₃ QDs in ambient and the vdW heterojunction interface between CsPbCl₃ QDs and graphene, leading to 73% photocurrent enhancement, three orders of magnitude improvement in response speed, and long term ambient stability [5]. In addition, light-assisted interface cleaning can provide a nondestructive approach to interface cleaning and can be combined with other methods for interface engineering [119]. It should be mentioned that these post-cleaning methods are particularly suitable and useful when the devices are fabricated by inkjet printing of QDs on graphene. In fact, printing with inks of pre-fabricated crystalline ODs [2, 22] or precursors that only require a moderate thermal budget [77, 120] compatible with silicon-based integrated circuits (Si-ROIC) provides a promising approach for integration of nanostructured devices with complementary metal oxide semiconductors (CMOS) [121]. Improvements of optoelectronic performance by orders of magnitudes have been reported when a clean vdW interface is achieved in QD/graphene photodetectors [2, 20, 104, 122].

3. Fabrication of QD/graphene vdW Heterostructures Photodetectors

3.1. Colloidal Synthesis of Quantum Dots

Colloidal techniques developed over the past three decades can produce monodisperse quantum dots (QDs) from diverse materials. Section 3.1.1 introduces the generalized process of colloidal QD synthesis, discusses how QD properties are determined during synthesis and summarizes common synthetic methods. Section 3.1.2 discusses recent developments and ongoing challenges in colloidal QD synthesis.

3.1.1 Basics of Colloidal Synthesis of Quantum Dots

Most widely-used methods of colloidal QD synthesis proceed through the homogeneous nucleation and growth mechanism first described by LaMer and Dinegar.[123, 124] The LaMer model includes three stages, and QD final properties are determined by the duration of each stage and the rates of several competing processes (**Fig. 6**). The initial reaction solution contains precursors of metal and anion species in the presence of coordinating ligands. Stage I begins with decomposition of precursors to generate solvated crystal monomers. When monomer concentration reaches some critical supersaturation, Stage II begins with the onset of spontaneous QD nucleation. The coordinating ligands prevent QD coalescence or bulk deposition but allow QD growth via monomer diffusion. QD nucleation and growth reduces the solution monomer concentration below supersaturation, halting nucleation and ending Stage II. In Stage III, QDs grow by collecting monomers from solution until reactants are consumed or the reaction is quenched.

Synthetic control of QD size, morphology, crystallinity and heterostructure (including surface properties) is achieved by selection of reagents and reaction conditions. QD monodispersity requires a temporally discrete nucleation event (Stage II), typically controlled through reaction temperature [123, 124]. QD size may be selected by quenching growth or by controlling the concentration of precursor and the rate of nucleation. The rate of nucleation is determined by reaction temperature and chemistry, particularly precursor and ligand design [32, 33, 125]. QD morphology and crystallinity are controlled via precursor stoichiometry and reaction conditions, and by designing ligands and precursors that favor formation and growth of specific phases or along particular crystalline planes [33-40]. Control of the chemical and electrical properties of QD surfaces poses a continuing challenge and has been addressed through reagent design, reaction conditions and core/shell heterostructures [32, 36, 39].

The hot-injection (HI) method described in 1993 by Murray et. al. is now the most common process for synthesizing high-quality 'conventional' (chalcogenide and III-V compounds) binary or multinary QDs [32, 38, 39, 124]. In HI synthesis, a precursor solution is rapidly heated by injection into a hot organic solvent, triggering precursor decomposition and Stage I of the LaMer model. Early HI methods followed Murray et. al.'s 'TOPO' route, using trioctylphosphine (TOP) as a solvent, trioctylphosphine oxide (TOPO) as a ligand, organometallic precursors and reaction temperatures from 100° to 300°C [41, 124]. Subsequent advances in reaction chemistry and control extended HI methods to new materials and structures, as discussed in 3.1.2. Drawbacks to HI synthesis include the toxicity of precursors, difficulty of controlling the injection step, and need for high temperature reactions under inert gases [36].

To avoid problems associated with the injection step, 'heat-up' and low temperature methods use careful modulation of reactor temperature to control QD nucleation and growth [33, 41, 42]. To circumvent cost and toxicity issues from organic solvents, aqueous routes have been developed for a wide variety of chalcogenide QDs, based on the early work on thiol-capped II-VI QDs by Rajh et al. and later Rogach et al [126, 127]. Compared to organic solvents, aqueous routes are more complex mechanistically due to the involvement of H⁺, OH⁻ and H₂O species and, to date, generally produce lower-quality QDs [41, 42].

Metal-halide perovskite QDs are an emerging class of promising optical materials. Compared to 'conventional' (group V- and VI-based) QD compounds, bonding in perovskites is less covalent and more ionic in character and perovskites have a higher solubility in typical polar organic HI solvents [43]. Since 2015, ligand-assisted reprecipitation (LARP) has replaced HI as the synthetic route of choice for perovskite QDs [6, 36, 43, 44, 128, 129]. In the LARP method, supersaturation

and nucleation is achieved by injecting precursors, dissolved in a good solvent, into a poor solvent in the presence of ligands.

Synthetic methods including solvothermal, emulsion, spray, vapor and plasma techniques do not follow the LaMer mechanism. Challenges such as experimental complexity and QD quality have limited the wider application of these methods [36, 39, 45].

3.1.2 Recent Progress in Colloidal QD Synthesis for Photodetection Applications

Research on QDs is driven by applications in fields including LEDs, solar power, biology and photodetectors. Further details are available in recent reviews.[32-48] The following discussion is restricted to photodetection applications and divided into two categories. Improvements to QD functionality address the electronic (e.g. charge transfer, bandgap...) and physical (e.g. stability, monodispersity...) properties of QDs. Improvements to manufacturability address factors limiting wider QD usage, such as toxicity and reaction scalability.

Advances in QD functionality typically improve existing QD materials or expand the range of accessible materials and structures. These advances are tied to reaction chemistry, particularly development of novel precursors and elucidating the mechanisms and kinetics governing QD formation. [36, 38-41, 125, 130-132] Of note, Owens and coworkers tuned the size and size distribution of PbS and PbSe QDs by manipulating the structures of thiourea and selenourea precursors.[125, 133] Other tunable precursors include diorganyl dichalcogenides and secondary phosphine sulfides.[39] Plasmonic QDs comprising nonstoichiometric nanocrystals have been produced by tuning precursor chemistry or the ratio of precursors.[24, 125]

Multinary QD heterostructures can combine desirable properties of different materials. Coreshell QDs may feature a core with desired 'bulk' properties (e.g. bandgap, absorption coefficient) and one or more shells with advantageous interfacial properties (e.g. charge transfer, passivation) [32, 36, 42, 43, 134]. Alternatively, interfacial properties may be exploited, such as plasmon-exciton coupling using a metal core and perovskite shell [135]. Adjusting precursor stoichiometry and reactivity in a one-step reaction can generate composition gradients in the radial direction, giving a surface enriched in one component [136-138]. Core-shell QDs with composition gradients or discreet interfaces may be generated by fed-batch operation or seeded growth followed by annealing [37, 38, 41, 48]. Seeded growth allows the combination of diverse materials, such as perovskites and metals or metal oxides.[36, 135] These techniques, as well as post-synthetic ion exchange, have also been used for QD doping [32, 38, 44, 131, 136, 139].

QD manufacturability is currently limited by challenges with scaling reactions to produce large volumes of uniform QDs, and by the toxicity of materials, particularly heavy metals and organometallic precursors [140, 141]. Cadmium- and lead-free perovskites have attracted attention as potential low-cost and low-toxicity QDs [36, 38, 42-44]. Aqueous routes continue to be a focus in the search for 'green' QDs.[32, 42] Mass- and heat-transfer present limitations to scaling of batch reactions, so scale-up efforts involve process intensification or alternative processes [45]. Goubet *et al* reported gram-scale production of HgTe QDs using concentrated precursors including liquid mercury [142]. Continuous microfluidic and flow-chemistry reactors are being examined as alternative synthetic processes [45, 141, 143, 144].

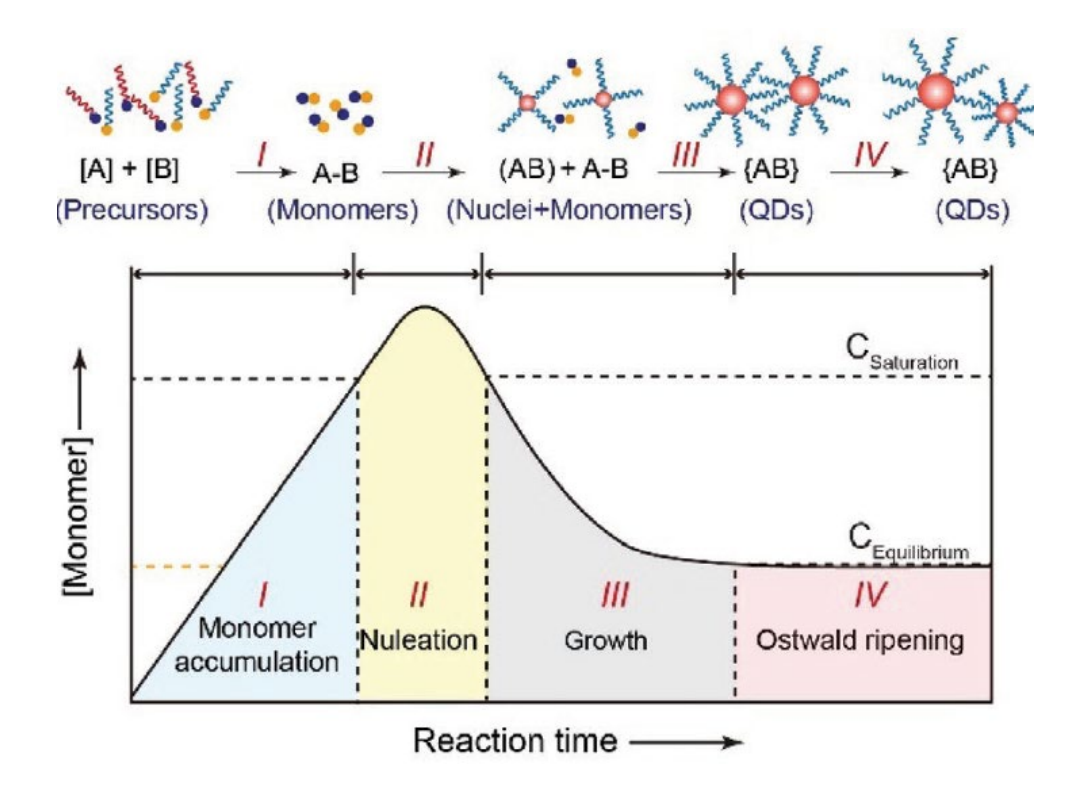


Fig. 6 Schematic and Lamer plot for the reaction in a wet-chemistry synthesis of nanocrystals. It contains four stages: (I) monomer accumulation, (II) nucleation, (III) growth and (IV) Ostwald ripening. Reproduced with permission.[11] Copyright 2020, John Wiley and Sons.

3.2. Chemical Vapor Deposition of Graphene

3.2.1. Chemical Vapor Deposition of Graphene on Metal Foils

Chemical vapor deposition (CVD) is considered a scalable and low cost approach for growth of graphene in the large areas required for graphene-based electronics, photonics and optoelectronics. In fact, the success in large-area growth of monolayer CVD graphene on Cu and other metal foils has made an important technological advance towards such applications [17, 145-147]. Cu has been particularly interesting since it has low solubility of carbon to prevent precipitation of carbon during the post-CVD cooling, which could lead to formation of multilayer graphene. While Cu foils are available in large area at a fairly low cost, they are usually polycrystalline and covered with a surface layer of CuO_x. In addition, most commercial Cu foils also have traces of oxygen in the bulk. This means the presence of H₂ during CVD growth of graphene is crucial for reduction of CuO_x and prevention of the formation of carbon oxides and other defects on CVD graphene [148, 149]. Cu can catalyze decomposition of the hydrocarbon used as the CVD source at the surface of the Cu foil to promote graphene nucleation, which occurs simultaneously on multiple sites on the Cu surface.⁵⁴ The follow-up growth of graphene is predominantly lateral along the edges of the graphene nuclei. Merging of neighboring graphene flakes is typically [17] through formation of defective grain boundaries (GBs). Fig. 7 illustrates images of such GBs using aberration-corrected annular dark-field scanning transmission electron microscopy (ADF-STEM) [150]. On GBs, an aperiodic line of defects stitching the two graphene grains together can be observed (Fig. 7c), on which are pentagons, heptagons and distorted hexagons. This is anticipated

since the orientations of the graphene nuclei occur randomly on polycrystalline Cu foils, resulting in lattice mismatch at the GBs. These GBs, together with damages and defects formed on graphene during the follow-up transfer from Cu foils to relevant substrates [151] result in a considerably reduced charge mobility in CVD graphene as compared to that for intrinsic graphene [151-154]. While monolayer is the dominant choice for electronic, photonic and optoelectronic devices, bilayer and multilayer graphene can find wide applications when other requirements, such as high electrical and thermal conductance, bandgap tunability, etc. are important. Through controlling of the CVD conditions, CVD graphene with desired layer numbers, such as ab-stacked bilayer graphene [155] and multilayer graphene have been obtained [146, 147, 156-158].

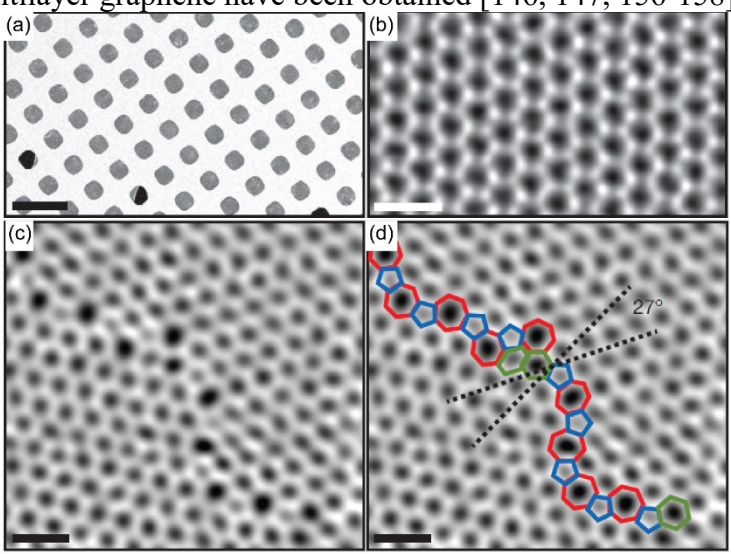


Fig. 7 (a)SEM image of graphene transferred onto a TEM grid with over 90% coverage. Scale bar: 5 μ m. (b) ADF-STEM image howing the defect-free hexagonal lattice inside a graphene grain. (c) Two grains (bottom left, top right) intersect with a 27 degree relative rotation. An aperiodic line of defects stitches the two grains together. (d) The image from c with the pentagons (blue), heptagons (red) and distorted hexagons (green) of the grain boundary outlined. b—d were low-pass-filtered to remove noise; scale bars, 5A°. Reprinted with permission. [147] Copyright 2011, Springer Nature.

3.2.2. Direct Growth of Graphene on Dielectric Substrates

The detrimental effect of GBs has motivated research in epitaxy of graphene on (111) oriented single-crystalline Cu foils or Cu thin films on single-crystalline substrates (quartz, Si, MgO, sapphire) and promising results have been reported [159-165]. However, scaling up these substrates may not be viable currently. Growth of graphene on nano-crystalline Cu foils, such as cubic textured (100) orientation Cu (CTO-Cu) substrates, is promising since CTO-Cu foils are available in large area at low cost. In comparison of graphene grains on polycrystalline Cu and CTO-Cu, it was found that the presence of sub-surface oxygen causes reconstruction of the Cu surface due to the formation of oriented Cu₂O nanocrystallites at a low H₂ gas flow. Self-assembly of the Cu₂O nanocrystallites into a textured surface template provides direct nucleation sites for graphene growth after the oxygen-sublattice on the template surface is reduced [166, 167]. The atomic Cu surface layer provides advantages of high graphene growth rate due to the catalytic role of Cu and in-plane alignment of graphene nuclei. It is particularly important that the Cu₂O crystallites predominantly have the (111) orientation aligned to each other in the plane of the (100) CTO-Cu substrates, which allows epitaxy of graphene with much lower defect, such as GBs, density as compared to that in the poly-Cu case. The considerably decreased GB density results in

both enhanced conductivity and transparency [166, 167]. Since Cu₂O (111) templates may be developed on lattice matched (100) surfaces of other dielectric materials, this self-assembly approach may provide a promising pathway for transfer free graphene epitaxy on nonmetallic surfaces.

Direct growth of graphene on dielectric substrates, such as SiO₂/Si, will allow elimination of the cumbersome graphene transfer process [168-177]. An early success was to obtain high quality graphene via sublimation of Si on crystalline SiC substrates at temperatures exceeding 1200 °C in high vacuum [176]. Compared to its CVD counterpart on metal foils, the graphene on SiC contains defects due to surface steps formed as a consequence of the surface recrystallization during the Si sublimation at high temperatures. In addition, SiC is expensive and cannot be used directly as gates for graphene field effect transistors. This motivated exploration of CVD of graphene directly on commercial SiO₂/Si substrates. Through a careful control of the CVD conditions, monolayer, bilayer and multilayer graphene has been obtained on large wafers of SiO₂/Si as well as transparent fused silica and quartz substrates [177]. Different from the transferred graphene, a cleaner interface was reported when a MoS₂ layer was grown on top of the graphene transfer-free graphene, leading to more efficient charge transfer across the MoS₂/graphene vdW interface and improved photoresponse and response speed [178, 179].

3.3. Fabrication of the QD/graphene vdW Heterostructures Photodetectors

3.3.1 Spin-Coating of QDs on Graphene

Colloidal QDs exhibit noticeably advantages in fabrication of QD/graphene vdW heterostructure photodetectors since QDs can be deposited on graphene using spin-coating [180]. This method can obtain a relative uniform thin film on different substrates, and the film thickness and morphology are tunable by adjusting the QDs concentration, spinning speed and number of layers.[181] After drying in inert gas atmosphere, tens to hundreds of nanometer thick QD active layers will be obtained. The process consists of dropping of a colloidal QDs solution on top of the graphene channel surface, which is fixed on a spin-coater compatible substrate. The colloidal QD solution can be dropped on the graphene channel before spinning or at the low spinning speed, depending on the nature of the QDs and solvents. Excess solvent will be removed by the centrifugal force and condensed films will be formed on the graphene surface. There is competition between viscous and centrifugal forces, therefore spinning speed plays a key role in the thickness of the QDs films. It is a good choice to suspend QDs in volatile solvents that can be easily removed and evaporated during the spinning process. There are several parameters that can tune and predict the thickness and uniformity of the films, such as QD concentration, viscosity of the solvent, spin speed, and rheology of the concentrating and solidifying suspension.[182] Colloidal ODs are especially suitable for spin-coating techniques for fabrication of QDs/graphene hybrid photodetectors.[180, 183] Spin-coated Si QDs on graphene channel have demonstrated high sensitivity photodetection.[184, 185] In addition, this method provides a non-destructive technique and can form the heterostructure on the surface of the graphene while preserving the high mobility of graphene charge transfer channels and enhancing the light absorption of the device. The processing versatility of this approach is particularly beneficial for top-surface photodetection systems, especially at room temperature and under ambient conditions.

In addition to the above advantages of the spin coating technique, there are also some limitations, such as mass scalability, target point fabrication, contamination on the fixed patterned electronic circuits, etc.

3.3.2 Inkjet printing of QDs on graphene

Inkjet printing is another emerging technique to construct QDs/graphene heterojunction structures, which exhibits unique advantage in low waste, low cost, mass scalability and especially direct deposition on a targeted area.[186] Calvert reviewed the growing efforts in inkjet printing for materials and devices.[187] An inkjet printer usually comprises an inkjet head, feeder rollers, and controller system. The inkjet head ejects QDs droplets in the patterned graphene channel. Feeder rollers feed QDs to the inkjet head and the controller system sets the printing image, position and drying heat energy.[182] Recently, an inkjet-printed heterostructure MoS₂/graphene photodetectors has been demonstrated on conformable substrates. that biocompatibility.[188] Finn et al reported all-printed photodetectors by printing of semiconducting MoS₂ nanosheets combined with inkjet-printed graphene interdigital array electrodes.[189] This approach allows photonic and high performance electronic components, based on functional nanomaterials prefabricated into highly crystalline nanostructures, to be incorporated with CMOS circuits with high or even unity fill factors for the development of compact and high resolution imaging systems.[180] To some extent, it can resolve the interconnection bottleneck that arises when further scaling down detector arrays whereas ongoing to enhance sensitivity and resolution. Inkjet printing techniques have the potential to be applied to QD/graphene heterostructure optoelectronic devices. The process of delivering the ink to the substrates is well-know. The issues as the ink interacts with the graphene channel require further study.

Fig. 8 shows a schematic of ZnO QDs printing process. ZnO QDs in ethanol were printed on GFETs using a SonoPlot microplotter through sonication of glass capillary tips.[2] The well-patterned GFET channels with 36 arrays were constructed on heavily doped Si (100) substrates with 90 nm of SiO₂ insulating layer. The ZnO QDs were suspended in ethanol solution and ultrasonicated before printing. Based on the size and position of the graphene channel, the printing process can be set and automatically deposited through software provided for lines, squares, circles, dots, and arch designs. The printed ZnO QDs form a condensed active layer on the top surface of graphene channel (**Fig.8c**). By systematically engineering the surface states of ZnO QDs, this hybrid ZnO QDs/GFET photodetector demonstrates extremely high photoconductive gain of 3.6×10^9 , photoresponsivity of 9.9×10^8 A/W and detectivity of 1×10^{14} Jones.

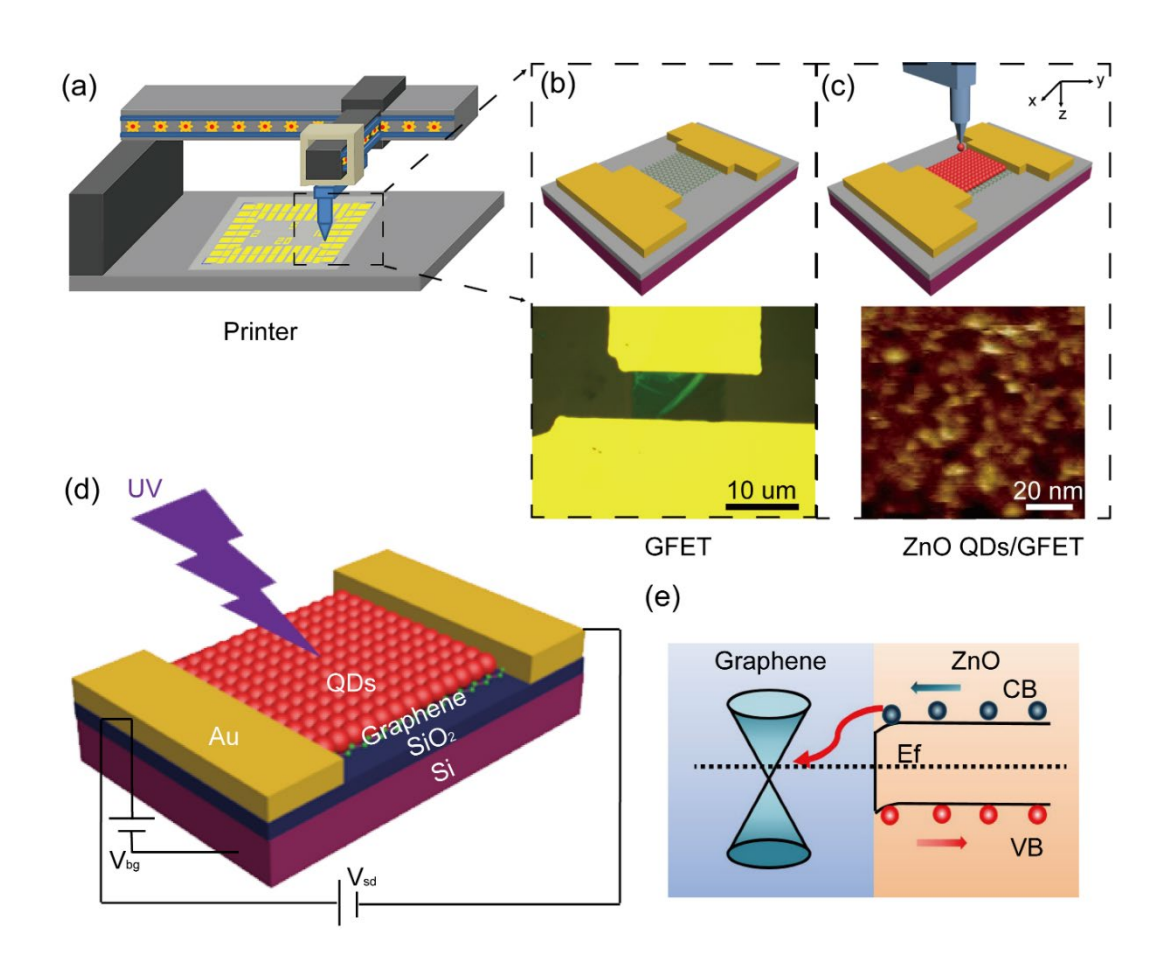


Fig. 8 Schematic image of ZnO QDs printing on patterned graphene channels. (a) Inkjet printer and a GFET array on Si/SiO₂ substrate. (b) A magnified view of a GFET device. (c) ZnO QDs were printed on the graphene channel (top) and AFM image was taken on the top of the ZnO QDs films. (d) Schematic of the ZnO QDs/GFET nanohybrid photodetectors. (e) Band energy edge of the ZnO QDs/graphene heterostructure and charges transport from ZnO QDs to graphene under illumination. Reprinted with permission. [2] Copyright 2017, American Chemical Society.

3.3.3. Growth of ODs on graphene

Transfer-free, wafer-size growth of photo sensitizers on graphene can provide a facile scheme for roll-to-roll fabrication of the vdW heterostructures photodetectors [114, 177]. A unique advantage of these directly grown heterostructures is an improved vdW interface that is critical to the charge transfer across the interface. For example, in MoS₂ nanodiscs on graphene heterostructure photodetectors (**Fig. 9**), Liu *et al* reported an order of magnitude enhancement in the photoresponsivity and two orders of magnitude faster photoresponse in devices made in a transfer-free layer- by-layer CVD method as compared to the similar devices made using transfer methods [114]. In addition to the CVD deposition of TMD nanostructure on graphene, Pradhan et al and Kim *et al* also reported direct growth of perovskite (CH₃NH₃PbBr) QDs and CdSe QDs on graphene, respectively, by casting corresponding precursors on graphene [18, 49]. It should be pointed out that direct growth may not universally solve the vdW interface problem since a poorquality interface may still form. For example, comparing a seedless and seeded growth of ZnO

NWs on GTC in a solution process [26], Cook *et al* have found the ZnO seed layer, typically with poor crystallinity, can provide strong charge trapping effect and therefore slow the photoresponse.

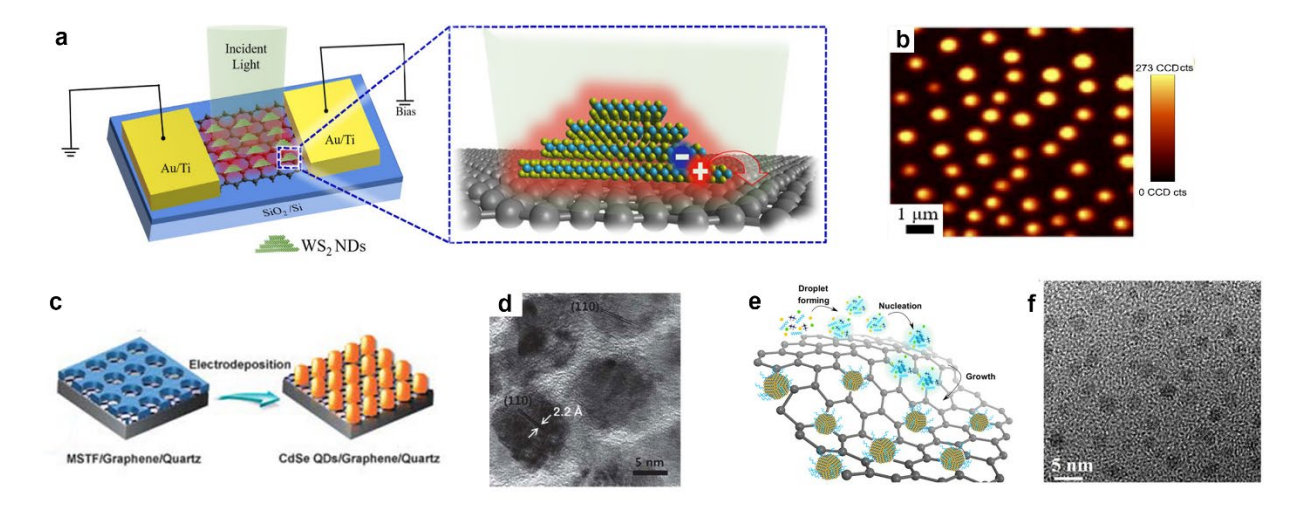


Fig. 9 (a) Schematic illustration of the photodetector based on WS2-NDs/graphene vdW heterostructure with WS₂-NDs directly grown on graphene. (b) $10 \times 10 \, \mu m^2$ Raman mapping images for E_{2g} peak of WS₂-NDs. Reproduced with permission.[10] Copyright 2019, American Chemical Society. (c) Schematic drawing of the procedure to fabricate CdSe QD directly on graphene. The fabrication includes the synthesis of an MSTF on the graphene on quartz, and electrodeposition of CdSe into the pores of the MSTF followed by the removal of MSTF which will leaves CdSe QDs on selected areas of graphene. (d) TEM image of CdSe QDs grown on graphene. Reproduced with permission.[18] Copyright 2012, RSC Publishing. (e) Schematic showing the growth of perovskite QDs on graphene; and (f) TEM image of the perovskite QDs distributed on the nanohybrid. Reproduced with permission.[49] Copyright 2020, American Association for the Advancement of Science.

4. Performance of the QD/Graphene vdW Heterostructures Photodetectors

After the first work of the PbS QDs/graphene IR detectors with high gains [20], QD/graphene vdW heterostructures have recently emerged as a promising scheme for high performance photodetectors. These QD/graphene vdW heterostructures take advantage of the strong quantum confinement in semiconductor QD photosensitizers with a much-enhanced light-matter interaction, spectral tunability well beyond the optical cutoff in bulk semiconductors, and reduced dark current due to suppressed phonon scattering [39, 75, 76], and of the extraordinary charge mobility in graphene for high EQE or gain up to 10^{10} - 10^{12} at room temperature [9, 13, 54, 55]. Many different QDs or even optical molecules have been used as photosensitizers in the QD/graphene vdW heterostructures for photodetection [2, 20, 104, 105, 190-194].

Tables 1-3 summarizes some representative results of QDs/graphene vdW heterostructure nanohybrids for infrared, visible and ultraviolet detection. For instance, Konstantatos *et al* reported a PbS/graphene nanohybrid photodetector with a layer of PbS QD as the tunable vis/IR absorber [12, 20]. The device worked under wavelength up to 1.6 μ m, and achieved D^* as high as 7×10^{13} Jones and response time of 10^{-2} s. In terms of visible detection, Kwak *et al* reported a high performance CsPbBr_{3-x}I_x perovskite NCs/graphene photodetector that has a detection range of 400 nm -700 nm and D^* of 10^{16} Jones [116]. As to UV detection, materials of quantum dots in the nanohybrid usually have wide bandgap, and ZnO is a typical material. For example, Gong et al

reported a printable ZnO QD/Graphene vdW heterostructures for ultrasensitive UV detection which achieved a D^* of 10^{13} Jones [2, 69].

Table 1. Performance of some representative QDs/graphene vdW heterostructures nanohybrid for infrared detection.

QD material	Detection	Cutoff	R	D* (Jones)	Response	Ref.
	region	wavelength	(A/W		time (s)	
	reported	(µm))			
PbS	Vis-SWIR	>1.8	-	10^{12} (at 1.55 µm)	10^{-3}	[12,
						31]
Ti ₂ O ₃	MWIR-	10	>120	7×10^{8} (at 10 µm)	10^{-3}	[195]
	LWIR					
HgTe	SWIR	1.55	6×10-	10^9 (at 1.55 µm)	9×10 ⁻⁶	[196]
			3	, ,		
HgTe	NIR-MIR	>3	10^{2}	$6 \times 10^8 (at 2.5 \mu m)$	7×10 ⁻⁴	[197]
Si (B-doped)	UV-MIR	3.9	10	$10^5 (at 3 \mu m)$	-	[185]
PbSe	NIR-MIR	3	7.6	-	2.8×10^{-4}	[198]
nanorods						

Table 2. Performance of QDs/graphene vdW heterostructures nanohybrid for visible light detection.

QD material	Detection region	Wavelength tested(nm)	R (A/W)	D* (Jones)	Response time (s)	Ref.
	reported				()	
PbS	Vis-	532	10^{7}	7×10^{13} (at 532 nm)	10^{-2}	[12]
	SWIR					
FeS ₂ /PbS	UV-NIR	500	3.27×10^6	$4.89 \times 10^{11} (at 500 nm)$	15	[199]
CdS	Vis	450	40	•	>80	[200]
PbS	UV-NIR	635	10^{7}	N/A	~5×10 ⁻²	[201]
Cu _{3-x} P	Vis-	405	9.34	$5.98 \times 10^{12} (at 405 nm)$	1	[202]
	SWIR					
CsPbBr ₃ -	Vis	400-700	8.2×10 ⁸	$2.4 \times 10^{16} (at 405 nm)$	3.65	[116]
$_{x}I_{x}$						_

Table 3. Performance of QDs/graphene vdW heterostructures nanohybrids for ultraviolet and high energy photon detection.

QD	Detection	Wavelength	R	D* (Jones)	Response	Ref.
material	region	tested(nm)	(A/W)		time (s)	
	reported					

ZnO	UV	300-400	9.9×10^{8}	7.5×10 ¹⁴ (at 340 nm)	5/85	[2, 203]
ZnO	UV	250-400	10^{8}	5.1×10^{13} (at 368 nm)	-	[204]
ZnSe/ZnS core/shell	UV	400	2×10^3	-	0.52	[205]
WS_2	UV	320-360	3.8×10^{3}	$1.6 \times 10^{13} (at 365 nm)$	2.04	[206]
ZrO ₂	UV	200-300	22	-	-	[207]
ZnS	UV	390	0.31	-	< 0.05	[208]
CsPbCl ₃	UV	300-400	10^{6}	10 ¹³ (at 390 nm)	0.3	[5]

QD/graphene nanohybrid photodetectors have been achieved with various functionalities (Fig. 10). For example, Gong et al reported a flexible CsPbCl₃ NCs/GFET photodetectors owing to the ink-based printable process-ability of QDs and the adaptability of graphene, and device performance was found to be unaffected after bending 25 times.[5] By purposely mixing two or more different QDs that prefer absorbing photons of different energy while having good energy band matches, it is easy to realize broadband photodetection. Gong *et al* reported a FeS₂ NCs-PbS QD/graphene nanohybrid photodetector, which combines the advantages of the high absorption coefficient of FeS₂ NCs and enhanced NIR absorption by PbS QDs to achieve high performance broadband photodetection.[199] Moreover, QD/graphene nanohybrids have great scalability to imagers by integrating with a readout circuit (ROICs). Konstantatos *et al* reported a broadband image sensor by integrating PbS QD/graphene nanohybrid to each pixel of a conventional CMOS die that served as light sensing units. [31]Due to NIR/SWIR absorption of former, this design removes limitation of conventional Si-based CMOS in visible region.

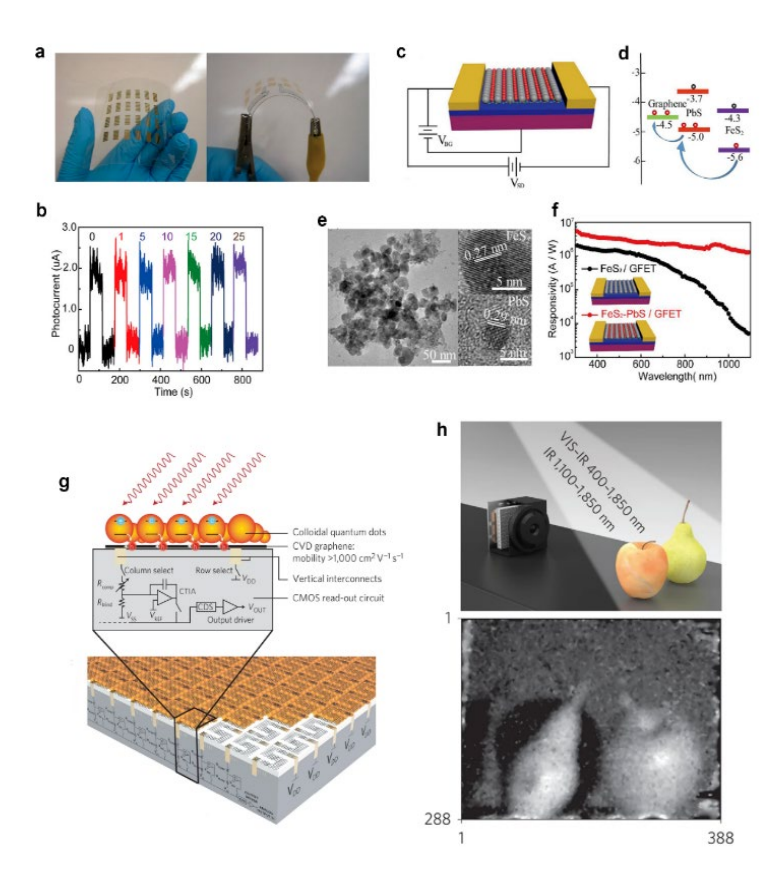


Fig. 10 (a) photos of flexible CsPbCl₃NCs/graphene device before and after bending. (b) Dynamic photoresponse after different numbers of bending cycles. Reproduced with permission.[5] Copyright 2019, American Chemistry Society. (c) Schematic image of the FeS₂–PbS/GFET nanohybrid photodetectors. The nanocomposite photosensitizer consists of FeS₂ NCs (gray) and PbS QDs (red). (d) Energy level diagram of the FeS₂–PbS/GFET heterojunction and charge transfer process under illumination. (e) TEM images of FeS₂–PbS nanocomposite (left) and the corresponding HRTEM images of FeS₂ NCs (upper right) and PbS QDs (lower right). (f) Spectral photoresponsivity of the FeS₂ NC–PbS QD/GFET and FeS₂ NC/GFET photodetectors under V_{DS} = 0.1 V. Reproduced with permission.[16] Copyright 2017, American Chemical Society. (g) Side view explaining the graphene photoconductor and the underlying read-out circuit. The graphene channels are sensitized to ultraviolet, visible, near-infrared and short-wave infrared light with PbS QDs. The bottom is the 3D impression of the monolithic image sensor displaying the top level with graphene carved into S-shaped channels sensitized with a layer of quantum dots, vertical interconnects and underlying CMOS read-out circuitry. (h) imaging set-up and near-infrared (NIR) and short-wave infrared (SWIR) light photograph of an apple and pear. Reproduced with permission.[31] Copyright 2017, Springer Nature.

5. Challenges remain and future perspectives

Despite progress made in research and development of QD/graphene vdW heterostructures photodetectors, challenges remain and must be addressed before commercial applications of these photodetectors. Scientifically, approaches for heterojunction interface engineering for more efficient exciton dissociation and charge transfer are needed for high-performance QD/graphene vdW heterostructures photodetectors. The challenge is that there may not be an approach which can be applied universally to all different QDs due to a diverse spectrum of QDs with different

surface states and optical spectrum for their applications. For example, ligand exchange has shown to be effective in passivating QD surface states and forming effective charge transfer pathways from OD to graphene in shorter wavelengths at which the ligands themselves will not exhibit any interference with the lights. At longer wavelengths, however, the light absorption by ligands could detrimentally affect the QD light absorption and charge transfer to graphene, resulting in difficulties in photodetection of MWIR or light with longer wavelengths. An additional challenge is in the quality of QD photosensitizers. Colloidal QDs can contain massive defects, especially on their surfaces. These surface states can lead to degradation of the QDs through reactions with molecules in the ambient, and in chemicals and solvents used for processing QDs. Furthermore, charge traps can form at these surface states or at the QD/graphene interface, resulting in reduced photo-generated carriers or photoresponse in photodetectors, and slow response speed. Passivation of the QD surface states using ligand caps or other approaches should be further explored. Finally, the difficulties to achieve device uniformity and yield in large scale present another challenge for commercialization. Therefore, it will remain as a major research focus in the future to achieve a better understanding and control of the optoelectronic process at multiple scales, from atomic to nanoscale, on the low-dimensional nanostructures and their heterojunction interfaces for light absorption, exciton dissociation and charge transfer, to device scale for charge transport with minimized charge recombination, in QD/graphene vdW heterostructures.

Acknowledgments

The authors acknowledge support in part by US ARO contract W911NF-16-1-0029, and US NSF contracts NSF-DMR-1508494, 1909292, and NSF-ECCS-1809293.

References

- 1. Liu, C.H., et al., *Graphene photodetectors with ultra-broadband and high responsivity at room temperature*. Nat Nanotechnol, 2014. **9**(4): p. 273-278.
- 2. Gong, M., et al., *All-Printable ZnO Quantum Dots/Graphene van der Waals Heterostructures for Ultrasensitive Detection of Ultraviolet Light*. ACS Nano, 2017. **11**: p. 4114-4123.
- 3. Sun, T., et al., Flexible Broadband Graphene Photodetectors Enhanced by Plasmonic Cu3-x P Colloidal Nanocrystals. Small, 2017. **13**(42): p. 1701881.
- 4. Jasieniak, J., M. Califano, and S.E. Watkins, *Size-Dependent Valence and Conduction Band-Edge Energies of Semiconductor Nanocrystals*. ACS Nano, 2011. **5**: p. 5888-5902.
- 5. Gong, M., et al., *High-Performance All-Inorganic CsPbCl3 Perovskite Nanocrystal Photodetectors with Superior Stability*. ACS Nano, 2019. **13**(2): p. 1772-1783.
- 6. Protesescu, L., et al., Nanocrystals of Cesium Lead Halide Perovskites (CsPbX(3), X = Cl, Br, and I): Novel Optoelectronic Materials Showing Bright Emission with Wide Color Gamut. Nano Lett, 2015. **15**(6): p. 3692-6.
- 7. Gong, M., et al., *Broadband Photodetectors Enabled by Localized Surface Plasmonic Resonance in Doped Iron Pyrite Nanocrystals*. Advanced Optical Materials, 2018. **6**(8): p. 1701241.
- 8. Novoselov, K.S., et al., *Electric field effect in atomically thin carbon films.* Science, 2004. **306**(5296): p. 666-669.
- 9. Geim, A.K. and K.S. Novoselov, The rise of graphene. Nature Materials, 2007. 6(3): p. 183-191.
- 10. Alamri, M., et al., *Plasmonic WS2 Nanodiscs/Graphene van der Waals Heterostructure Photodetectors*. ACS Appl Mater Interfaces, 2019. **11**(36): p. 33390-33398.
- 11. Chen, B., D. Li, and F. Wang, *InP Quantum Dots: Synthesis and Lighting Applications*. Small, 2020. **16**(32): p. e2002454.
- 12. Konstantatos, G., et al., *Hybrid graphene-quantum dot phototransistors with ultrahigh gain.* Nat Nanotechnol, 2012. **7**(6): p. 363-8.
- 13. Geim, A.K., *Graphene: Status and Prospects*. Science, 2009. **324**(5934): p. 1530-1534.
- 14. Tetsuka, H., A. Nagoya, and S.I. Tamura, *Graphene/nitrogen-functionalized graphene quantum dot hybrid broadband photodetectors with a buffer layer of boron nitride nanosheets.* Nanoscale, 2016. **8**(47): p. 19677-19683.
- 15. Gong, M., et al., Localized Surface Plasmon Resonance Enhanced Light Absorption in AuCu/CsPbCl3 Core/Shell Nanocrystals. Advanced Materials, 2020. **32**(26): p. 2002163.
- 16. Gong, M., et al., *Printable Nanocomposite FeS2-PbS Nanocrystals / Graphene Heterojunction Photodetectors for Broadband Photodetection.* ACS Appl Mater Interfaces, 2017. **9**: p. 27801–27808.
- 17. Li, X.S., et al., *Large-Area Synthesis of High-Quality and Uniform Graphene Films on Copper Foils.* Science, 2009. **324**(5932): p. 1312-1314.
- 18. Kim, Y.T., et al., Synthesis of a CdSe-graphene hybrid composed of CdSe quantum dot arrays directly grown on CVD-graphene and its ultrafast carrier dynamics. Nanoscale, 2013. **5**(4): p. 1483-8.
- 19. Wu, J.Z., *Graphene*, in *Transparent Conductive Materials. Materials, Synthesis and Characterization*, D.L.a.D.E. Castellón, Editor. 2019, Wiley-VCH. p. 165-192.
- 20. Konstantatos, G., et al., *Hybrid graphene-quantum dot phototransistors with ultrahigh gain.* Nature Nanotechnology, 2012. **7**(6): p. 363-368.
- 21. Geim, A.K. and I.V. Grigorieva, *Van der Waals heterostructures.* Nature, 2013. **499**(7459): p. 419-425.
- 22. Gong, M., Liu, Qingfeng, Cook, Brent, Ewing, Daniel, Casper, Matthew, Stramel, Wu, Judy *All-printable ZnO quantum dots/Graphene van der Waals heterostructures for ultrasensitive detection of ultraviolet light*. ACS nano, 2017. **11**(4): p. 4114.

- 23. Gong, M.G., et al., *High-Performance All-Inorganic CsPbCl3 Perovskite Nanocrystal Photodetectors with Superior Stability*. Acs Nano, 2019. **13**(2): p. 1772-1783.
- 24. Gong, M., et al., *Controllable Synthesis of Monodispersed Fe1- xS2 Nanocrystals for High-Performance Optoelectronic Devices.* ACS Appl Mater Interfaces, 2019. **11**(21): p. 19286-19293.
- 25. Gong, M., et al., Broadband Photodetectors: Broadband Photodetectors Enabled by Localized Surface Plasmonic Resonance in Doped Iron Pyrite Nanocrystals (Advanced Optical Materials 8/2018). Advanced Optical Materials, 2018. **6**(8): p. 1870033.
- 26. Cook, B., et al., Facile zinc oxide nanowire growth on graphene via a hydrothermal floating method: towards Debye length radius nanowires for ultraviolet photodetection. Journal of Materials Chemistry C, 2017. **5**(38): p. 10087-10093.
- 27. Liu, J., et al., Development of a Seedless Floating Growth Process in Solution for Synthesis of Crystalline ZnO Micro/Nanowire Arrays on Graphene: Towards High Performance Nanohybrid Ultraviolet Photodetectors. Advanced Functional Materials, 2013. **23**(39): p. 4941-4948.
- 28. Xia, F., et al., *Two-dimensional material nanophotonics*. Nature Photonics, 2014. **8**: p. 899-907.
- 29. Roy, K., et al., *Graphene–MoS2 hybrid structures for multifunctional photoresponsive memory devices.* Nature Nanotechnology, 2013. **8**: p. 826-830.
- 30. Alamri, M., et al., *Graphene/WS2 Nanodisk Van der Waals Heterostructures on Plasmonic Ag Nanoparticle-Embedded Silica Metafilms for High-Performance Photodetectors.* ACS Applied Nano Materials, 2020. **3**(8): p. 7858-7868.
- 31. Goossens, S., et al., *Broadband image sensor array based on graphene–CMOS integration*. Nature Photonics, 2017. **11**(6): p. 366-371.
- 32. Kovalenko, M.V., et al., *Prospects of nanoscience with nanocrystals.* ACS Nano, 2015. **9**(2): p. 1012-57.
- 33. Murray, C.B., et al., *Colloidal synthesis of nanocrystals and nanocrystal superlattices*. IBM Journal of Research and Development, 2001. **45**(1): p. 47-56.
- 34. Sablon, K.A., et al., *High-response hybrid quantum dots- 2D conductor phototransistors: recent progress and perspectives.* Nanophotonics, 2017. **6**(6): p. 1263-1280.
- 35. Talapin, D.V., et al., *Prospects of colloidal nanocrystals for electronic and optoelectronic applications*. Chem Rev, 2010. **110**(1): p. 389-458.
- 36. Chen, K., et al., *The chemistry of colloidal semiconductor nanocrystals: From metal-chalcogenides to emerging perovskite.* Coordination Chemistry Reviews, 2020. **418**.
- 37. Owen, J. and L. Brus, *Chemical Synthesis and Luminescence Applications of Colloidal Semiconductor Quantum Dots.* J Am Chem Soc, 2017. **139**(32): p. 10939-10943.
- 38. Ma, Y., Y. Zhang, and W.W. Yu, *Near infrared emitting quantum dots: synthesis, luminescence properties and applications.* Journal of Materials Chemistry C, 2019. **7**(44): p. 13662-13679.
- 39. Lu, H., et al., *Infrared Quantum Dots: Progress, Challenges, and Opportunities.* ACS Nano, 2019. **13**(2): p. 939-953.
- 40. Evans, C.M., et al., *Review of the synthesis and properties of colloidal quantum dots: the evolving role of coordinating surface ligands.* Journal of Coordination Chemistry, 2012. **65**(13): p. 2391-2414
- 41. Green, M. and H. Mirzai, *Synthetic routes to mercury chalcogenide quantum dots.* Journal of Materials Chemistry C, 2018. **6**(19): p. 5097-5112.
- 42. Jing, L., et al., Aqueous Based Semiconductor Nanocrystals. Chem Rev, 2016. **116**(18): p. 10623-730.
- 43. Akkerman, Q.A., et al., *Genesis, challenges and opportunities for colloidal lead halide perovskite nanocrystals*. Nat Mater, 2018. **17**(5): p. 394-405.
- 44. Shamsi, J., et al., *Metal Halide Perovskite Nanocrystals: Synthesis, Post-Synthesis Modifications, and Their Optical Properties.* Chem Rev, 2019. **119**(5): p. 3296-3348.

- 45. Pu, Y., et al., *Colloidal Synthesis of Semiconductor Quantum Dots toward Large-Scale Production: A Review.* Industrial & Engineering Chemistry Research, 2018. **57**(6): p. 1790-1802.
- 46. García de Arquer, F.P., et al., *Solution-processed semiconductors for next-generation photodetectors.* Nature Reviews Materials, 2017. **2**(3).
- 47. Murray, C.B., C.R. Kagan, and M.G. Bawendi, *Synthesis and Characterization of Monodisperse Nanocrystals and Close-Packed Nanocrystal Assemblies*. Annual Review of Materials Science, 2000. **30**(1): p. 545-610.
- 48. Shu, Y., et al., *Quantum Dots for Display Applications*. Angew Chem Int Ed Engl, 2020. **59**(50): p. 22312-22323.
- 49. Pradhan, B., et al., *Ultrasensitive and ultrathin phototransistors and photonic synapses using perovskite quantum dots grown from graphene lattice.* Sci Adv, 2020. **6**(7): p. eaay5225.
- 50. Novoselov, K.S., et al., *Electric field effect in atomically thin carbon films.* Science, 2004. **306**(5696): p. 666-669.
- 51. Novoselov, K.S., et al., *Two-dimensional gas of massless Dirac fermions in graphene*. Nature, 2005. **438**(7065): p. 197-200.
- 52. Zhang, Y.B., et al., Experimental observation of the quantum Hall effect and Berry's phase in graphene. Nature, 2005. **438**(7065): p. 201-204.
- 53. Avouris, P., Z.H. Chen, and V. Perebeinos, *Carbon-based electronics*. Nature Nanotechnology, 2007. **2**(10): p. 605-615.
- 54. Dean, C.R., et al., *Boron nitride substrates for high-quality graphene electronics*. Nature Nanotechnology, 2010. **5**(10): p. 722-726.
- 55. Chen, J.H., et al., *Intrinsic and extrinsic performance limits of graphene devices on SiO2*. Nature Nanotechnology, 2008. **3**(4): p. 206-209.
- 56. Bockelmann, U., *ELECTRONIC RELAXATION IN QUASI-ONE-DIMENSIONAL AND ZERO-DIMENSIONAL STRUCTURES.* Semiconductor Science and Technology, 1994. **9**(5): p. 865-870.
- 57. Kuo, D.M.T., A.B. Fang, and Y.C. Chang, *Theoretical modeling of dark current and photo-response* for quantum well and quantum dot infrared detectors. Infrared Physics & Technology, 2001. **42**(3-5): p. 433-442.
- 58. Logeeswaran, V.J., et al., *A Perspective on Nanowire Photodetectors: Current Status, Future Challenges, and Opportunities.* leee Journal of Selected Topics in Quantum Electronics, 2011. **17**(4): p. 1002-1032.
- 59. Keuleyan, S., et al., *Mid-infrared HgTe colloidal quantum dot photodetectors*. Nature Photonics, 2011. **5**(8): p. 489-493.
- 60. Keuleyan, S., E. Lhuillier, and P. Guyot-Sionnest, *Synthesis of Colloidal HgTe Quantum Dots for Narrow Mid-IR Emission and Detection.* Journal of the American Chemical Society, 2011. **133**(41): p. 16422-16424.
- 61. Lhuillier, E., et al., *Thermal properties of mid-infrared colloidal quantum dot detectors.* Journal of Applied Physics, 2011. **110**(3).
- 62. Chen, H., et al., *Infrared Detection Using an InSb Nanowire*, in *2009 IEEE Nanotechnology Materials and Devices Conference*. 2009: Traverse City, Michigan, USA. p. 212.
- 63. Khan, M.I., et al., *Study of a Single InSb Nanowire Fabricated via DC Electrodeposition in Porous Templates*. Journal of Nanoscience and Nanotechnology, 2009. **9**(4): p. 2639-2644.
- 64. Liu, Q., et al., Fused Nanojunctions of Electron Depleted ZnO Nanoparticles for Extraordinary Performance in Ultraviolet Detection. Advanced Materials Interfaces, 2017.
- 65. Roy, S., et al., *Investigation of Charge Transfer Interactions in CdSe Nanorod P3HT/PMMA Blends by Optical Microscopy.* Journal of Physical Chemistry C, 2012. **116**(4): p. 3153-3160.
- 66. Zhang, W.J., et al., *Ultrahigh-Gain Photodetectors Based on Atomically Thin Graphene-MoS2 Heterostructures.* Scientific Reports, 2014. **4**: p. 3826.

- 67. Zhang, W.J., et al., *High-Gain Phototransistors Based on a CVD MoS2 Monolayer*. Advanced Materials, 2013. **25**(25): p. 3456-3461.
- 68. Lu, R.T., Liu, J. W., Luo, H. F., Chikan, V., and Wu, J. Z., *Ligand-Free Graphene/GaSe-Nanosheet Hybrid: Towards High Gain and Fast Photoresponse.* submitted., 2015.
- 69. Gong, M., Liu, Qingfeng, Cook, Brent, Ewing, Daniel, Casper, Matthew, Stramel, Wu, Judy *All-printable ZnO quantum dots/Graphene van der Waals heterostructures for ultrasensitive detection of ultraviolet light, ASAP.* ACS NANO, ASAP, 2017.
- 70. Zheng, K.H., et al., *Visible Photoresponse of Single-Layer Graphene Decorated with TiO2 Nanoparticles*. Small, 2013. **9**(12): p. 2076-2080.
- 71. Liu, J.W., et al., Development of a Seedless Floating Growth Process in Solution for Synthesis of Crystalline ZnO Micro/Nanowire Arrays on Graphene: Towards High-Performance Nanohybrid Ultraviolet Photodetectors. Advanced Functional Materials, 2013. **23**(39): p. 4941-4948.
- 72. Echtermeyer, T.J., et al., *Strong plasmonic enhancement of photovoltage in graphene*. Nature Communications, 2011. **2**: p. 458.
- 73. Liu, Y., et al., *Plasmon resonance enhanced multicolour photodetection by graphene.* Nature Communications, 2011. **2**: p. 579.
- 74. Xu, G., et al., Photodetection based on Ionic Liquid Gated Plasmonic Ag Nanoparticle/ Graphene Nanohybrid Field Effect Transistors. Advanced Optical Materials, 2014. **2**(8): p. 729-736.
- 75. Tang, J., et al., *Colloidal-quantum-dot photovoltaics using atomic-ligand passivation*. Nature Materials, 2011. **10**(10): p. 765-771.
- 76. Ip, A.H., et al., *Hybrid passivated colloidal quantum dot solids.* Nat Nanotechnol, 2012. **7**(9): p. 577-82.
- 77. Cook, B., et al., *Quantum Dots-Facilitated Printing of ZnO Nanostructure Photodetectors with Improved Performance*. Acs Applied Materials & Interfaces, 2017. **9**(27): p. 23189-23194.
- 78. Cook., B., Gong, M.G., Ewing, D., Casper, M., Stramel, A., Elliot, A., Wu, J.Z., *Inkjet-Printing Multi-Color Pixilated Quantum Dots on Graphene for Broadband Photodetection.* ACS Applied Nano Materials, 2019. **2**: p. 3246.
- 79. Wu, J.Z., *Graphene*, in *Transparent Conductive Materials. Materials, Synthesis and Characterization*, D.L.a.D.E. Castellón, Editor. 2018, Wiley-VCH.
- 80. Bonaccorso, F., et al., *Graphene photonics and optoelectronics*. Nature Photonics, 2010. **4**(9): p. 611-622.
- 81. Wu, J., *Graphene*, in *Transparent Conductive Materials*. 2019. p. 165-192.
- 82. Nair, R.R., et al., *Fine structure constant defines visual transparency of graphene.* Science, 2008. **320**(5881): p. 1308-1308.
- 83. De, S. and J.N. Coleman, *Are There Fundamental Limitations on the Sheet Resistance and Transmittance of Thin Graphene Films?* Acs Nano, 2010. **4**(5): p. 2713-2720.
- 84. Stankovich, S., et al., *Graphene-based composite materials*. Nature, 2006. **442**(7100): p. 282-286.
- 85. Nair, R.R., et al., *Fine structure constant defines visual transparency of graphene.* Science, 2008. **320**(5881): p. 1308.
- 86. Wassei, J.K. and R.B. Kaner, *Graphene, a promising transparent conductor*. Materials Today, 2010. **13**(3): p. 52-59.
- 87. Xia, F.N., et al., *Two-dimensional material nanophotonics*. Nature Photonics, 2014. **8**(12): p. 899-907.
- 88. Matyba, P., et al., *Graphene and Mobile Ions: The Key to All-Plastic, Solution-Processed Light-Emitting Devices.* Acs Nano, 2010. **4**(2): p. 637-642.
- 89. Mueller, T., F.N.A. Xia, and P. Avouris, *Graphene photodetectors for high-speed optical communications*. Nature Photonics, 2010. **4**(5): p. 297-301.

- 90. Lin, Y.M., et al., 100-GHz Transistors from Wafer-Scale Epitaxial Graphene. Science, 2010. **327**(5966): p. 662-662.
- 91. Bunch, J.S., et al., *Electromechanical resonators from graphene sheets*. Science, 2007. **315**(5811): p. 490-493.
- 92. Stoller, M.D., et al., Graphene-Based Ultracapacitors. Nano Letters, 2008. 8(10): p. 3498-3502.
- 93. Liu, Z.F., et al., *Organic Photovoltaic Devices Based on a Novel Acceptor Material: Graphene.* Advanced Materials, 2008. **20**(20): p. 3924.
- 94. Luther, J.M., et al., Localized surface plasmon resonances arising from free carriers in doped quantum dots. Nature Materials, 2011. **10**(5): p. 361-366.
- 95. Gordon, R.G., Criteria for choosing transparent conductors. Mrs Bulletin, 2000. 25(8): p. 52-57.
- 96. Orlita, M. and M. Potemski, *Dirac electronic states in graphene systems: optical spectroscopy studies.* Semiconductor Science and Technology, 2010. **25**(6): p. 063001.
- 97. Kravets, V.G., et al., Spectroscopic ellipsometry of graphene and an exciton-shifted van Hove peak in absorption. Physical Review B, 2010. **81**(15): p. 155413.
- 98. Nelson, F.J., et al., *Optical properties of large-area polycrystalline chemical vapor deposited graphene by spectroscopic ellipsometry.* Applied Physics Letters, 2010. **97**(25): p. 253110.
- 99. Wang, K., et al., Synthesis and photovoltaic effect of vertically aligned ZnO/ZnS core/shell nanowire arrays. Applied Physics Letters, 2010. **96**(12): p. 123105.
- 100. Weber, J.W., V.E. Calado, and M.C.M. van de Sanden, *Optical constants of graphene measured by spectroscopic ellipsometry*. Applied Physics Letters, 2010. **97**(9): p. 091904.
- 101. Xia, F.N., et al., *Ultrafast graphene photodetector*. Nature Nanotechnology, 2009. **4**(12): p. 839-843.
- 102. Fujita, M., et al., *Peculiar localized state at zigzag graphite edge.* Journal of the Physical Society of Japan, 1996. **65**(7): p. 1920-1923.
- 103. Kosynkin, D.V., et al., *Longitudinal unzipping of carbon nanotubes to form graphene nanoribbons.* Nature, 2009. **458**(7240): p. 872-U5.
- 104. Gong, M.G., et al., *Printable Nanocomposite FeS2-PbS Nanocrystals/Graphene Heterojunction Photodetectors for Broadband Photodetection.* Acs Applied Materials & Interfaces, 2017. **9**(33): p. 27801-27808.
- 105. Gong, M., et al., Broadband Photodetectors: Broadband Photodetectors Enabled by Localized Surface Plasmonic Resonance in Doped Iron Pyrite Nanocrystals (Advanced Optical Materials 8/2018). Advanced Optical Materials, 2018. **6**(8).
- 106. Lu, R.T., Liu, J. W., Luo, H. F., Chikan, V., and Wu, J. Z., *Graphene/GaSe-Nanosheet Hybrid: Towards High Gain and Fast Photoresponse.* Scientific Reports, 2016. **6**: p. 19161.
- 107. Meera, V. and G.S. Setlur, *Ellipsometry of graphene on a substrate*. Journal of Applied Physics, 2010. **107**(3): p. 033525.
- 108. Stoberl, U., et al., *Morphology and flexibility of graphene and few-layer graphene on various substrates.* Applied Physics Letters, 2008. **93**(5): p. 051906.
- 109. Wu, J., et al., *The Interaction between Quantum Dots and Graphene: The Applications in Graphene Based Solar Cells and Photodetectors.* Advanced Functional Materials, 2018. **28**(50).
- 110. Xu, G.W., et al., *Plasmonic Graphene Transparent Conductors*. Advanced Materials, 2012. **24**(10): p. OP71-OP76.
- 111. Lu, R.T., Konxelmann, A., Xu, F., Gong, Y.P., Liu, J.W., Liu, Q.F., Xin, M., Hui, R., Wu, J.Z., *High Sensitivity Surface Enhanced Raman Spectroscopy of Rhodamine 6G on in situ Fabricated Au-Nanoparticle/Graphene Plasmonic Substrates*. Carbon, 2015(online available doi: 10.1016/j.carbon.2015.01.028).

- 112. Liu, B., et al., *Using Silver Nanoparticles-Embedded Silica Metafilms as Substrates to Enhance the Performance of Perovskite Photodetectors.* ACS Applied Materials & Interfaces, 2019. **11**(35): p. 32301-32309.
- 113. Xu, G.W., et al., Photodetection Based on Ionic Liquid Gated Plasmonic Ag Nanoparticle/Graphene Nanohybrid Field Effect Transistors. Advanced Optical Materials, 2014. **2**(8): p. 729-736.
- 114. Liu, Q.F., Cook, B., Gong, M.G., Gong, Y.P., Ewing, D., Casper, M., Stramel, A., Wu, J.Z.,, *Transfer-Free Fabrication of Two-Dimensional MoS2/Graphene Heterostructures on SiO2/Si Substrates for High-Performance and Scalable Photodetectors.* ACS Applied Materials & Interfaces, 2017. **9**(14): p. 12728.
- 115. Rogalski, A., Infrared Detectors (Second Edition). 2011, Boca Raton, FL: CRC Press.
- 116. Kwak, D.-H., et al., *High performance hybrid graphene–CsPbBr3–xlx perovskite nanocrystal photodetector*. RSC Advances, 2016. **6**(69): p. 65252-65256.
- 117. Ma, C., et al., Detangling extrinsic and intrinsic hysteresis for detecting dynamic switch of electric dipoles using graphene field-effect transistors on ferroelectric gates. Nanoscale (cover article), 2015. **7**: p. 18489-18497.
- 118. Turyanska, L., et al., Ligand Induced Control of Photoconductive Gain and Doping in a Hybrid Graphene Quantum Dot Transistor. Advanced Electronic Materials, 2015. **1**(7).
- Hu, G.L., et al., *Self-Organization of Ions at the Interface between Graphene and Ionic Liquid DEME-TFSI.* Acs Applied Materials & Interfaces, 2017. **9**(40): p. 35437-35443.
- 120. Liu, Q.F., et al., *Transfer-free and printable graphene/ZnO-nanoparticle nanohybrid photodetectors with high performance.* Journal of Materials Chemistry C, 2017. **5**(26): p. 6427-6432.
- 121. Kim, J., et al., Advanced Materials for Printed Wearable Electrochemical Devices: A Review. Advanced Electronic Materials, 2017. **3**(1).
- 122. Lu, R., et al., *Graphene/GaSe-Nanosheet Hybrid: Towards High Gain and Fast Photoresponse.* Scientific reports, 2016. **6**.
- 123. LaMer, V.K. and R.H. Dinegar, *Theory, Production and Mechanism of Formation of Monodispersed Hydrosols*. Journal of the American Chemical Society, 1950. **72**(11): p. 4847-4854.
- 124. Murray, C.B., D.J. Norris, and M.G. Bawendi, *Synthesis and characterization of nearly monodisperse CdE (E = sulfur, selenium, tellurium) semiconductor nanocrystallites.* Journal of the American Chemical Society, 1993. **115**(19): p. 8706-8715.
- 125. Hendricks, M.P., et al., NANOMATERIALS. A tunable library of substituted thiourea precursors to metal sulfide nanocrystals. Science, 2015. **348**(6240): p. 1226-30.
- 126. Rajh, T., O.I. Micic, and A.J. Nozik, *Synthesis and characterization of surface-modified colloidal cadmium telluride quantum dots.* The Journal of Physical Chemistry, 1993. **97**(46): p. 11999-12003.
- 127. Rogach, A., et al., *Colloidally Prepared HgTe Nanocrystals with Strong Room-Temperature Infrared Luminescence*. Advanced Materials, 1999. **11**(7): p. 552-555.
- 128. Zhang, F., et al., *Brightly Luminescent and Color-Tunable Colloidal CH3NH3PbX3 (X = Br, I, Cl) Quantum Dots: Potential Alternatives for Display Technology.* ACS Nano, 2015. **9**(4): p. 4533-42.
- 129. Li, X., et al., CsPbX3Quantum Dots for Lighting and Displays: Room-Temperature Synthesis, Photoluminescence Superiorities, Underlying Origins and White Light-Emitting Diodes. Advanced Functional Materials, 2016. **26**(15): p. 2435-2445.
- 130. Peng, Z.A. and X. Peng, Formation of high-quality CdTe, CdSe, and CdS nanocrystals using CdO as precursor. J Am Chem Soc, 2001. **123**(1): p. 183-4.
- 131. Berends, A.C., et al., *Interplay between Surface Chemistry, Precursor Reactivity, and Temperature Determines Outcome of ZnS Shelling Reactions on CulnS2 Nanocrystals.* Chem Mater, 2018. **30**(7): p. 2400-2413.

- 132. Kershaw, S.V., et al., Development of Synthetic Methods to Grow Long-Wavelength Infrared-Emitting HgTe Quantum Dots in Dimethylformamide. Chemistry of Materials, 2020. **32**(9): p. 3930-3943.
- 133. Campos, M.P., et al., *A Library of Selenourea Precursors to PbSe Nanocrystals with Size Distributions near the Homogeneous Limit.* J Am Chem Soc, 2017. **139**(6): p. 2296-2305.
- 134. Shen, G. and P. Guyot-Sionnest, *HgTe/CdTe and HgSe/CdX (X = S, Se, and Te) Core/Shell Mid-Infrared Quantum Dots.* Chemistry of Materials, 2018. **31**(1): p. 286-293.
- 135. Gong, M., et al., Localized Surface Plasmon Resonance Enhanced Light Absorption in AuCu/CsPbCl3 Core/Shell Nanocrystals. Adv Mater, 2020. **32**(26): p. e2002163.
- 136. Shen, G., M. Chen, and P. Guyot-Sionnest, *Synthesis of Nonaggregating HgTe Colloidal Quantum Dots and the Emergence of Air-Stable n-Doping.* J Phys Chem Lett, 2017. **8**(10): p. 2224-2228.
- 137. Yang, H., et al., Design Rules for One-Step Seeded Growth of Nanocrystals: Threading the Needle between Secondary Nucleation and Ripening. Chemistry of Materials, 2019. **31**(11): p. 4173-4183.
- 138. Cai, W., et al., *High quality CdHgTe nanocrystals with strong near-infrared emission: relationship between composition and cytotoxic effects.* Langmuir, 2013. **29**(12): p. 4119-27.
- 139. De Trizio, L. and L. Manna, *Forging Colloidal Nanostructures via Cation Exchange Reactions*. Chem Rev, 2016. **116**(18): p. 10852-87.
- 140. Livache, C., et al., *Road Map for Nanocrystal Based Infrared Photodetectors*. Front Chem, 2018. **6**: p. 575.
- 141. Lignos, I., R. Maceiczyk, and A.J. deMello, *Microfluidic Technology: Uncovering the Mechanisms of Nanocrystal Nucleation and Growth.* Acc Chem Res, 2017. **50**(5): p. 1248-1257.
- 142. Goubet, N., et al., *Near- to Long-Wave-Infrared Mercury Chalcogenide Nanocrystals from Liquid Mercury.* The Journal of Physical Chemistry C, 2020. **124**(15): p. 8423-8430.
- 143. Kubendhiran, S., et al., *Microfluidic Synthesis of Semiconducting Colloidal Quantum Dots and Their Applications*. ACS Applied Nano Materials, 2019. **2**(4): p. 1773-1790.
- Sui, J., et al., *Continuous Synthesis of Nanocrystals via Flow Chemistry Technology.* Small, 2020. **16**(15): p. e1902828.
- 145. Kim, K.S., et al., *Large-scale pattern growth of graphene films for stretchable transparent electrodes.* Nature, 2009. **457**(7230): p. 706-710.
- 146. Liu, W., et al., Controllable and Rapid Synthesis of High-Quality and Large-Area Bernal Stacked Bilayer Graphene Using Chemical Vapor Deposition. Chemistry of Materials, 2014. **26**(2): p. 907-915.
- 147. Wu, Y.P., et al., *Growth Mechanism and Controlled Synthesis of AB-Stacked Bilayer Graphene on Cu-Ni Alloy Foils.* Acs Nano, 2012. **6**(9): p. 7731-7738.
- 148. Vlassiouk, I., et al., *Role of Hydrogen in Chemical Vapor Deposition Growth of Large Single-Crystal Graphene*. Acs Nano, 2011. **5**(7): p. 6069-6076.
- 149. Bhaviripudi, S., et al., *Role of Kinetic Factors in Chemical Vapor Deposition Synthesis of Uniform Large Area Graphene Using Copper Catalyst.* Nano Letters, 2010. **10**(10): p. 4128-4133.
- 150. Huang, P.Y., et al., *Grains and grain boundaries in single-layer graphene atomic patchwork quilts.* Nature, 2011. **469**(7330): p. 389-+.
- 151. Rochford, C., et al., *All-Optical Technique to Correlate Defect Structure and Carrier Transport in Transferred Graphene Films*. Acs Applied Materials & Interfaces, 2013. **5**(15): p. 7176-7180.
- 152. Li, X.S., et al., *Transfer of Large-Area Graphene Films for High-Performance Transparent Conductive Electrodes.* Nano Letters, 2009. **9**(12): p. 4359-4363.
- 153. Rochford, C., et al., *The effect of annealing on the photoconductivity of carbon nanofiber/TiO2 core-shell nanowires for use in dye-sensitized solar cells.* Applied Physics Letters, 2010. **97**(4): p. 043102.

- 154. Bae, S., et al., *Roll-to-roll production of 30-inch graphene films for transparent electrodes.* Nature Nanotechnology, 2010. **5**(8): p. 574-578.
- 155. Liu, Q.F., et al., Synchronous growth of AB-stacked bilayer graphene on Cu by simply controlling hydrogen pressure in CVD process. Carbon, 2015. **93**: p. 199-206.
- 156. Liu, L.X., et al., *High-Yield Chemical Vapor Deposition Growth of High-Quality Large-Area AB-Stacked Bilayer Graphene*. Acs Nano, 2012. **6**(9): p. 8241-8249.
- 157. Yan, K., et al., Formation of Bilayer Bernal Graphene: Layer-by-Layer Epitaxy via Chemical Vapor Deposition. Nano Letters, 2011. **11**(3): p. 1106-1110.
- 158. Luo, Z.Q., et al., *Large-Scale Synthesis of Bi-layer Graphene in Strongly Coupled Stacking Order.*Advanced Functional Materials, 2011. **21**(5): p. 911-917.
- 159. Sutter, P., J.T. Sadowski, and E. Sutter, *Graphene on Pt(111): Growth and substrate interaction.* Physical Review B, 2009. **80**(24): p. 245411.
- 160. Sutter, P.W., P.M. Albrecht, and E.A. Sutter, *Graphene growth on epitaxial Ru thin films on sapphire*. Applied Physics Letters, 2010. **97**(21): p. 213101.
- 161. Ismach, A., et al., *Direct chemical vapor deposition of graphene on dielectric surfaces*. Nano Letters, 2010. **10**(5): p. 1542-1548.
- Levendorf, M.P., et al., *Transfer-free batch fabrication of single layer graphene transistors.* Nano Letters, 2009. **9**(12): p. 4479-4483.
- 163. Ago, H., et al., *Patterned growth of graphene over epitaxial catalyst.* Small, 2010. **6**(11): p. 1226-1233.
- 164. Reddy, K.M., et al., *High quality, transferable graphene grown on single crystal Cu(111) thin films on basal-plane sapphire.* arXiv:1012.1588v1 2010.
- 165. Gao, L., J.R. Guest, and N.P. Guisinger, *Epitaxial graphene on Cu(111)*. Nano Lett, 2010. **10**(9): p. 3512-6.
- 166. Liu, J., et al., Role of Cu surface nanostructure on nucleation of graphene. preprint, 2011.
- 167. Liu, J.W., et al., *Direct graphene growth on (111) Cu2O templates with atomic Cu surface layer.* Carbon, 2015. **95**: p. 608-615.
- 168. Sun, J., et al., Controllable chemical vapor deposition of large area uniform nanocrystalline graphene directly on silicon dioxide. Journal of Applied Physics, 2012. **111**(4).
- 169. Bi, H., et al., *Direct growth of few-layer graphene films on SiO2 substrates and their photovoltaic applications.* Journal of Materials Chemistry, 2012. **22**(2): p. 411-416.
- 170. Hong, G., et al., *Mechanism of non-metal catalytic growth of graphene on silicon*. Applied Physics Letters, 2012. **100**(23): p. 231604.
- 171. Zhang, L., et al., *Catalyst-free growth of nanographene films on various substrates.* Nano Research, 2011. **4**(3): p. 315-321.
- Wei, D.P. and X.F. Xu, *Laser direct growth of graphene on silicon substrate*. Applied Physics Letters, 2012. **100**(2): p. 023110.
- 173. Tian, S.B., et al., *Robust adhesion of flower-like few-layer graphene nanoclusters*. Scientific Reports, 2012. **2**: p. 511.
- 174. Medina, H., et al., *Metal-Free Growth of Nanographene on Silicon Oxides for Transparent Conducting Applications*. Advanced Functional Materials, 2012. **22**(10): p. 2123-2128.
- 175. Chen, J.Y., et al., *Oxygen-Aided Synthesis of Polycrystalline Graphene on Silicon Dioxide Substrates.*Journal of the American Chemical Society, 2011. **133**(44): p. 17548-17551.
- 176. Kedzierski, J., Hsu, P., Healey, P., Wyatt, P., Keast, C., Sprinkle, M., Berger, C., de Heer, W., , *Epitaxial graphene transistors on SiC substrates.* IEEE Transactions on Electron Devices 2008. **55**: p. 2078.

- 177. Liu, Q.F., Gong, Y.P., Wang, T., Chan, W.L., Wu, J.Z., *Metal-catalyst-free and controllable synthesis of monolayer, bilayer and few-layer graphene on silicon dioxide by chemical vapor deposition.* Carbon, 2015. **96**: p. 203.
- 178. Liu, Q.F., et al., *Printable Transfer-Free and Wafer-Size MoS2/Graphene van der Waals Heterostructures for High-Performance Photodetection*. Acs Applied Materials & Interfaces, 2017. **9**(14): p. 12728-12733.
- 179. Alamri, M., et al., *Plasmonic WS2 Nanodiscs/Graphene van der Waals Heterostructure Photodetectors*. ACS Applied Materials & Interfaces, 2019. **11**(36): p. 33390-33398.
- 180. García de Arquer, F.P., et al., *Solution-processed semiconductors for next-generation photodetectors*. Nature Reviews Materials, 2017. **2**(3): p. 16100.
- 181. Liang, Z., et al., Effects of the Morphology of a ZnO Buffer Layer on the Photovoltaic Performance of Inverted Polymer Solar Cells. Advanced Functional Materials, 2012. **22**(10): p. 2194-2201.
- 182. Li, C., et al., Recent advances in solution-processed photodetectors based on inorganic and hybrid photo-active materials. Nanoscale, 2020. **12**(4): p. 2201-2227.
- 183. Shin, D.H. and S.H. Choi, *Graphene-Based Semiconductor Heterostructures for Photodetectors.* Micromachines (Basel), 2018. **9**(7).
- 184. Yu, T., et al., *Graphene Coupled with Silicon Quantum Dots for High-Performance Bulk-Silicon-Based Schottky-Junction Photodetectors*. Adv Mater, 2016. **28**(24): p. 4912-9.
- 185. Ni, Z., et al., *Plasmonic Silicon Quantum Dots Enabled High-Sensitivity Ultrabroadband Photodetection of Graphene-Based Hybrid Phototransistors.* ACS Nano, 2017. **11**(10): p. 9854-9862.
- 186. Cook, B., et al., *Inkjet Printing Multicolor Pixelated Quantum Dots on Graphene for Broadband Photodetection*. ACS Applied Nano Materials, 2019. **2**(5): p. 3246-3252.
- 187. Calvert, P., Inkjet Printing for Materials and Devices. Chem. Mater., 2001. 13: p. 3299-3305.
- 188. Hossain, R.F., et al., *Biocompatible, large-format, inkjet printed heterostructure MoS2-graphene photodetectors on conformable substrates.* npj 2D Materials and Applications, 2017. **1**(1).
- 189. Finn, D.J., et al., *Inkjet deposition of liquid-exfoliated graphene and MoS2nanosheets for printed device applications*. J. Mater. Chem. C, 2014. **2**(5): p. 925-932.
- 190. Sun, Z.H., et al., *Infrared Photodetectors Based on CVD-Grown Graphene and PbS Quantum Dots with Ultrahigh Responsivity*. Advanced Materials, 2012. **24**(43): p. 5878-5883.
- 191. Zhang, D.Y., et al., *Understanding Charge Transfer at PbS-Decorated Graphene Surfaces toward a Tunable Photosensor*. Advanced Materials, 2012. **24**(20): p. 2715-2720.
- 192. Gong, M., et al., *Iron Pyrite (FeS2) Broad Spectral and Magnetically Responsive Photodetectors.* Advanced Optical Materials, 2013. **1**(1): p. 78-83.
- 193. Gong, M.G., Adhikaru, P., Gong, Y.P., Wang, To, Liu, Q.F., Kafle, B., Ching, W.Y., Chan, W.L., Wu, J.Z., , *Polarity Controlled Attachment of Cytochrome C for High Performance Cytochrome C/Graphene van der Waals Heterojunction Photodetectors*. Advanced Functional Materials 2018. **28**.
- 194. Liu, B., et al., Cation— π Interaction Assisted Molecule Attachment and Photocarrier Transfer in Rhodamine/Graphene Heterostructures. Advanced Materials Interfaces, 2020. **7**(16): p. 2000796.
- 195. Yu, X., et al., *Narrow bandgap oxide nanoparticles coupled with graphene for high performance mid-infrared photodetection.* Nat Commun, 2018. **9**(1): p. 4299.
- 196. Noumbe, U.N., et al., *Reconfigurable 2D/OD p-n Graphene/HgTe Nanocrystal Heterostructure for Infrared Detection*. ACS Nano, 2020. **14**(4): p. 4567-4576.
- 197. Grotevent, M.J., et al., *Colloidal HgTe Quantum Dot/Graphene Phototransistor with a Spectral Sensitivity Beyond 3 μm.* Advanced Science, 2021.
- 198. Talebi, H., et al., *Fabrication of fast mid-infrared range photodetector based on hybrid graphene-PbSe nanorods.* Appl Opt, 2015. **54**(20): p. 6386-90.

- 199. Gong, M., et al., *Printable Nanocomposite FeS2-PbS Nanocrystals/Graphene Heterojunction Photodetectors for Broadband Photodetection.* ACS Appl Mater Interfaces, 2017. **9**(33): p. 27801-27808.
- 200. Chan, Y., et al., Fabrication of hybrid graphene/CdS quantum dots film with the flexible photodetecting performance. Physica E: Low-dimensional Systems and Nanostructures, 2020. **124**.
- 201. Ahn, S., et al., *Optoelectronic response of hybrid PbS-QD/graphene photodetectors.* J Chem Phys, 2019. **151**(23): p. 234705.
- 202. Sun, T., et al., Flexible Broadband Graphene Photodetectors Enhanced by Plasmonic Cu3-x P Colloidal Nanocrystals. Small, 2017. **13**(42).
- 203. Gong, M., et al., All-Printable ZnO Quantum Dots/Graphene van der Waals Heterostructures for Ultrasensitive Detection of Ultraviolet Light. ACS Nano, 2017. **11**(4): p. 4114-4123.
- 204. Shao, D., et al., *Organic-Inorganic Heterointerfaces for Ultrasensitive Detection of Ultraviolet Light*. Nano Lett, 2015. **15**(6): p. 3787-92.
- 205. Sun, Y.L., et al., *Hybrid graphene/cadmium-free ZnSe/ZnS quantum dots phototransistors for UV detection.* Sci Rep, 2018. **8**(1): p. 5107.
- 206. Singh, V.K., et al., *WS2 Quantum Dot Graphene Nanocomposite Film for UV Photodetection.* ACS Applied Nano Materials, 2019. **2**(6): p. 3934-3942.
- 207. Shi, X., X. Liu, and H. Zeng, *ZrO 2 quantum dots/graphene phototransistors for deep UV detection.* Materials Research Bulletin, 2017. **96**: p. 458-462.
- 208. Premkumar, S., et al., *Highly Responsive Ultraviolet Sensor Based on ZnS Quantum Dot Solid with Enhanced Photocurrent*. Sci Rep, 2019. **9**(1): p. 18704.